JOURNAL OF GEOPHYSICAL RESEARCH, VOL. 107, NO. D24, 8217, doi:10.1029/2001JD000881, 2002

Correction published 18 February 2003

Validation and data characteristics of water vapor profiles observed by the Improved Limb Atmospheric Spectrometer (ILAS) and processed with the version 5.20 algorithm

H. Kanzawa,[1] C. Schiller,[2] J. Ovarlez,[3] C. Camy-Peyret,[4] S. Payan,[4] P. Jeseck,[4] H. Oelhaf,[5] M. Stowasser,[5] W. A. Traub,[6] K. W. Jucks,[6] D. G. Johnson,[6,7] G. C. Toon,[8] B. Sen,[8] J.-F. Blavier,[8] J. H. Park,[9] G. E. Bodeker,[10] L. L. Pan,[11] T. Sugita,[1] H. Nakajima,[1] T. Yokota,[1] M. Suzuki,[1,12] M. Shiotani,[13,14] and Y. Sasano[1]

Received 24 May 2001; revised 5 November 2001; accepted 27 November 2001; published 31 December 2002.

[1] Vertical profiles of water vapor concentration at high latitudes (57–72°N; 64–89°S) were observed by the Improved Limb Atmospheric Spectrometer (ILAS) solar occultation sensor aboard the Advanced Earth Observing Satellite (ADEOS). These measurements were made continuously from November 1996 through June 1997 with some additional periods in September to October 1996. A validation study of the water vapor data processed with the version 5.20 ILAS retrieval algorithm is presented in this paper. Uncertainty and general characteristics of the ILAS water vapor measurements are briefly reviewed. Comparisons are made with data obtained by (1) the ILAS validation balloon campaigns at Kiruna, Sweden and at Fairbanks, Alaska; (2) the aircraft measurements under the Photochemistry of Ozone Loss in the Arctic Region in Summer (POLARIS) campaign; and (3) available satellite measurements of the version 19 Halogen Occultation Experiment (HALOE) and the version 6 Stratospheric Aerosol and Gas Experiment II (SAGE II). The agreement between ILAS water vapor and all independent reliable correlative measurements in the altitude region of 15–60 km is better than 10% for the majority of cases and better than 20% for all comparisons, with the exception of some isolated cases detailed in this paper. Climatological comparisons of ILAS data with Upper Atmosphere Research Satellite (UARS) climatology and HALOE data show the overall consistency of ILAS water vapor data considering the known features of atmospheric circulation. The characteristics of ILAS measurements, i.e., high sampling frequency in polar latitudes with high vertical resolution along with the good data quality, make the ILAS water vapor data set valuable for various polar stratospheric research applications. *INDEX TERMS:* 0340 Atmospheric Composition and Structure: Middle atmosphere—composition and chemistry; 0341 Atmospheric Composition and Structure: Middle atmosphere—constituent transport and chemistry (3334); 0365 Atmospheric Composition and Structure: Troposphere—composition and chemistry; 0368 Atmospheric Composition and Structure: Troposphere—constituent transport and chemistry; 3334 Meteorology and Atmospheric Dynamics: Middle atmosphere dynamics (0341, 0342); *KEYWORDS:* water vapor, polar stratosphere, validation, satellite sensor, Improved Limb Atmospheric Spectrometer (ILAS)

Citation: Kanzawa, H., et al., Validation and data characteristics of water vapor profiles observed by the Improved Limb Atmospheric Spectrometer (ILAS) and processed with the version 5.20 algorithm, *J. Geophys. Res.*, *107*(D24), 8217, doi:10.1029/2001JD000881, 2002.

[1]National Institute for Environmental Studies, Tsukuba, Japan.
[2]Institut für Stratosphaerische Chemie, Forschungszentrum Jülich, Germany.
[3]Laboratoire de Météorologie Dynamique/Centre National de la Recherche Scientifique, Palaiseau, France.
[4]Laboratoire de Physique Moléculaire et Applications, Université Pierre et Marie Curie/Centre National de la Recherche Scientifique, Paris, France.
[5]Institut für Meteorologie und Klimaforschung, Forschungszentrum Karlsruhe, Germany.
[6]Harvard-Smithsonian Center for Astrophysics, Cambridge, Massachusetts, USA.
[7]Now at NASA Langley Research Center, Hampton, Virginia, USA.
[8]Jet Propulsion Laboratory, California Institute of Technology, Pasadena, California, USA.
[9]NASA Langley Research Center, Hampton, Virginia, USA.
[10]National Institute of Water and Atmospheric Research, Lauder, New Zealand.
[11]National Center for Atmospheric Research, Boulder, Colorado, USA.
[12]Now at National Space Development Agency of Japan/Earth Observation Research Center, Tokyo, Japan.
[13]Graduate School of Environmental Earth Science, Hokkaido University, Sapporo, Japan.
[14]Now at Radio Science Center for Space and Atmosphere, Kyoto University, Kyoto, Japan.

0148-0227/02/2001JD000881

1. Introduction

[2] There are two main sources of water vapor in the stratosphere: (1) Water vapor is injected from the troposphere into the stratosphere mainly through the equatorial tropopause and transported upward and poleward; (2) Water vapor is produced by oxidation of methane in the upper stratosphere and mesosphere. Water vapor in the stratosphere is important directly in two aspects, i.e., radiative and chemical. Radiatively, water vapor is the most important greenhouse gas [e.g., *Harries*, 1996] while chemically, water vapor is strongly related to ozone chemistry through HOx chemistry and through its role as a source of PSCs (Polar Stratospheric Clouds) [e.g., *Solomon*, 1999]. Water vapor is also important indirectly as a driver of dynamical motion in the stratosphere, which is basically induced by radiative heating/cooling determined from the distribution of water vapor as well as ozone and carbon dioxide [e.g., *Andrews et al.*, 1987]. The distribution of water vapor in the stratosphere is determined by the interaction of radiation, chemistry, and dynamics. The phase of stratospheric water vapor can be liquid or solid depending on whether it is incorporated into aerosols or various types of PSC. Water vapor is transported downward in the stratospheric polar vortex which forms in the winter season.

[3] Water vapor is considered as a long-lived tracer and analysis of its distribution therefore provides insights into stratospheric dynamics and transport. An example is to give a view of the atmospheric ''tape recorder'', i.e., water vapor is used as a tracer for estimating vertical velocities in the equatorial lower stratosphere [e.g., *Mote et al.*, 1996]. Some data indicated that water vapor has increased since the 1980s up to now in the stratosphere [e.g., *Oltmans and Hofmann*, 1995; *Oltmans et al.*, 2000; *Rosenlof et al.*, 2001]. In view of the significance of water vapor in the upper troposphere and stratosphere, the WCRP-SPARC (Stratospheric Processes and their Role in Climate) project carried out the Water Vapour Assessment (WAVAS) [*Kley et al.*, 2000].

[4] Satellite measurements of water vapor are very useful for investigating water vapor behavior in the stratosphere. The first instrument that produced a global distribution of water vapor in the stratosphere was the LIMS (Limb Infrared Monitor of the Stratosphere) on board the Nimbus 7 satellite [e.g., *Gille and Russell*, 1984; *Jones et al.*, 1986]. SAGE (Stratospheric Aerosol and Gas Experiment) II succeeded LIMS for conducting water vapor measurements [e.g., *Rind et al.*, 1993; *McCormick et al.*, 1993; *Chiou et al.*, 1997]. HALOE (Halogen Occultation Experiment) and MLS (Microwave Limb Sounder) on board UARS (Upper Atmosphere Research Satellite) provide data sets of water vapor as well as other species [e.g., *Harries et al.*, 1996; *Lahoz et al.*, 1996]. We use SAGE II, HALOE, and MLS data for comparison in this paper. POAM (Polar Ozone and Aerosol Measurement) III is the latest instrument to measure water vapor [e.g., *Lucke et al.*, 1999]. All these satellite data are used in the WAVAS report [*Kley et al.*, 2000].

[5] The ILAS (Improved Limb Atmospheric Spectrometer) solar occultation instrument was developed by the Environment Agency (EA) of Japan (recently reorganized as the Ministry of the Environment (MOE)), and it was operated on board the Advanced Earth Observing Satellite (ADEOS) spacecraft of the National Space Development Agency (NASDA) of Japan [e.g., *Sasano et al.*, 1999a]. ILAS measured water vapor (H_2O) as well as other species of ozone (O_3), nitric acid (HNO_3), nitrogen dioxide (NO_2), nitrous oxide (N_2O), methane (CH_4), and aerosols. ILAS operated continuously from November 1996 to June 1997 with some additional periods in September and October 1996. ILAS version 4.20 H_2O data are included in the WAVAS report [*Kley et al.*, 2000].

[6] The validation analyses of ILAS O_3, HNO_3, and aerosol extinction coefficient at 780 nm gave good results for version 3.10 of the data processing algorithm [*Sasano et al.*, 1999b; *Lee et al.*, 1999; *Koike et al.*, 2000; *Burton et al.*, 1999; *Hayashida et al.*, 2000]. ILAS version 3.10 H_2O compared well with validation balloon data in the ILAS validation balloon campaign [*Sasano et al.*, 1999c], but had some shortcomings such as unreasonable oscillation with altitude above about 30 km. Moreover, the version 3.10 algorithm provided values larger than anticipated for N_2O and CH_4 in the lower stratosphere. Since there are some overlaps in ILAS infrared spectral measurements among H_2O, N_2O, and CH_4, the final retrieval results might interfere with each other.

[7] This paper is devoted to validating ILAS version 5.20 water vapor (H_2O) profiles, and to describing their data characteristics on the basis of various validation measurements of balloons, aircraft, and satellites. Using the ILAS version 5.20 water vapor data, *Pan et al.* [2002] discuss the variability of polar stratospheric water vapor and make climatological comparison of ILAS with the UARS (Upper Atmosphere Research Satellite) Reference Atmosphere climatology as a function of Ertel's potential vorticity (PV)-based equivalent latitude and potential temperature. As for other ILAS version 5.20 products, validation of long-lived tracers of nitrous oxide (N_2O) and methane (CH_4) is described in a companion paper H. Kanawa et al., Validation and data characteristics of nitrous oxide and methane profiles observed by the Improved Limb Atmospheric Spectrometer (ILAS) and processed with the version 5.20 algorithm, submitted to *Journal of Geophysical Research*, 2002. Other companion papers by *Sugita et al.* [2002], *Irie et al.* [2002], and *Saitoh et al.* [2002] discuss results of validation analyses of ozone (O_3), of nitrogen dioxide (NO_2) and nitric acid (HNO_3), and of aerosol extinction coefficient, respectively.

[8] Section 2 presents a brief summary of the ILAS measurements, the version 5.20 data processing algorithm, and error budget results, further details of which are described by *Yokota et al.* [2002] and *Nakajima et al.* [2002b]. Section 3 describes the overall ILAS data characteristics of water vapor. Section 4 describes the methods used for validation of ILAS water vapor. Section 5 presents validation analyses using balloonborne measurement data in the Arctic. Section 6 presents validation analyses using aircraft data of POLARIS in the Arctic. Section 7 compares ILAS water vapor profiles in the Arctic and the Antarctic with other coincident satellite measurements of HALOE and SAGE II, both of which use the same principle of solar occultation as ILAS. Section 8 compares the variability of monthly means of ILAS with that of the UARS Reference Atmosphere climatology and

HALOE. Section 9 summarizes the comparisons, and draws some conclusions.

2. Brief Summary of ILAS Measurement, Data Processing Algorithm, and Error Budget

[9] An overview of the ILAS measurements is given, e.g., by *Sasano et al.* [1999a]. A brief description of the ILAS instrument is given by *Suzuki et al.* [1995], and its detailed characteristics and performance are given by *Nakajima et al.* [2002a]. A concept of the algorithm to derive water vapor and other species concentrations from the ILAS infrared spectrometer measurements is shown in *Yokota et al.* [1998]. In this paper, the most recent complete release of data products, those processed by the version 5.20 algorithm, is used. A detailed description of the version 5.20 data processing algorithm is given by *Yokota et al.* [2002], and a description of the tangent height determination method is given by *Nakajima et al.* [2002b]. The operational data processing is carried out at ILAS DHF (Data Handling Facility) at NIES in Japan [e.g., *Kanzawa*, 1996]. Version 4.20 H_2O (released in July 1999) is also referred to because it was used in the SPARC/WAVAS report. Version 3.10 H_2O (released in November 1997) is also referred to because it was used in a simple comparison with validation measurements by *Sasano et al.* [1999c]. In this section, the ILAS measurement characteristics are briefly reviewed for the present purpose of H_2O validation.

[10] ILAS is a solar occultation sensor which consists of two grating spectrometers (covering 6.21–11.77 μm with a 44-spectral element pyroelectric array detector, and 0.753–0.784 μm with a 1024-spectral element metal-oxide-semiconductor (MOS) photodiode array detector, respectively) and a Sun edge sensor. The absorption around 6.5 μm is used for detecting water vapor molecules. The absorption line parameters used for the retrieval are from HITRAN96 [*Rothman et al.*, 1998]. The ILAS water vapor measurement is not expected to suffer strong interference from other gases although there are slight influences from CH_4 and N_2O. The O_2 collision-induced absorption around 6.4 μm also affects ILAS H_2O as discussed in *Yokota et al.* [2002].

[11] At the tangent point, the instantaneous field of view (IFOV) for the infrared (IR) spectrometer is 1.6 km high and 13 km wide. The partial slant path along the line of sight within a 1-km thick layer just above the tangent height (TH) of 20 km is approximately 230 km. With a sampling rate of 12 Hz, a full spectrum over the 44 IR spectral elements is acquired every 83 m s. The tangent height (TH) interval is about 110 m at a TH of 15 km and 270 m at a TH of 55 km when atmospheric refraction effects are taken into account. Time series smoothing, which corresponds to about 10 samplings, is applied in the transmittance data, so the actual vertical resolution is 1.9 km at a TH of 15 km, 2.5 km at 25 km, 3.0 km at 35 km, 3.4 km at 45 km, and 3.5 km at and above 55 km [*Yokota et al.*, 2002]. For reference, the vertical resolution of SAGE II and HALOE is estimated to be ~1 km and ~2 km, respectively. The ADEOS satellite was put into a Sun-synchronous polar orbit with an inclination angle of 98.6°, and with an equator crossing (descending) time of around 10:40 local mean solar time. Therefore the ILAS occultation events occur at sunrise and sunset seen from the ADEOS satellite on each of about 14 orbits per day. The measurement region of ILAS is over high latitudes (57–72°N and 64–89°S), as shown in Figure 1.

[12] Vertical profiling of atmospheric constituents is performed by using an onion-peeling retrieval method [*Yokota et al.*, 2002]. The retrieval altitude for water vapor ranges from 8 km (at the lowest) to 70 km as shown in Figures 1 and 2. The retrieval altitude grid interval is 1 km in geometric altitude. The unphysical oscillation in the vertical H_2O profiles has been improved in the version 5.20 data by applying a low-pass filter to suppress noise in processing level 0 data (original measurement) to level 1 data (pseudo-transmittance for detector elements). No artificial smoothing to the level 2 products (geophysical parameters such as water vapor) is applied.

[13] A summary of the error analyses for the version 5.20 ILAS water vapor data is shown in Table 1 (for details, see also *Yokota et al.* [2002]). The errors associated with the version 5.20 data are separated into two categories: internal and external. The internal errors refer to errors calculated from the final residuals after convergence of the nonlinear least squares fitting of the observed and simulated transmittances. The external errors refer to errors associated with the calculation of the simulated transmittance through uncertainties in the nongaseous component correction and temperature profiles, which are used as inputs to the retrieval. Note that the internal error includes terms affecting both precision (random error) and accuracy (systematic error plus random error), as does the external error. The total error is defined as the root-sum-square (RSS) of the internal and external errors. The total error and internal error are provided in each version 5.20 ILAS data file.

[14] The methods for deriving the external errors are described below. The nongaseous component correction [*Sasano et al.*, 1999a; *Yokota et al.*, 2002] is required in order to derive vertical profiles of the gaseous concentration in the altitude range where extinction due to aerosol particles, sulfate aerosols and/or Polar Stratospheric Clouds (PSCs), cannot be neglected. To determine the nongaseous contribution in the simulated transmittance, we first evaluate the extinction coefficient profiles due to the gaseous components at the 4 spectral elements where the absorption due to gaseous species is relatively small (so-called ''window spectral element''). To evaluate the gaseous contribution, we use profiles of O_3, HNO_3, NO_2, N_2O, CH_4, H_2O, CO_2, and other minor gaseous concentrations (such as CFC-11) from an ILAS reference atmosphere model [*Yokota et al.*, 2002]. Then, the nongaseous contribution is calculated by subtracting the gaseous one from the total extinction coefficient measured at each window element, and then they are linearly interpolated and extrapolated with wave number to give the nongaseous transmittance at all the other 40 spectral elements. The 44 spectral element transmittance data thus estimated are used to correct for the nongaseous contribution when deriving gas profiles. Use of data from the reference atmosphere model would induce some errors in the calculation of the simulated transmittance. The magnitude of these errors were estimated from simulations for suitably selected 32 sample measurements by employing profiles of 10 percentile, median, and 90 percentile values in these reference data. These errors are one of the components of the external errors. The interpolation would also produce systematic errors for the retrieved profiles of the gaseous concentration,

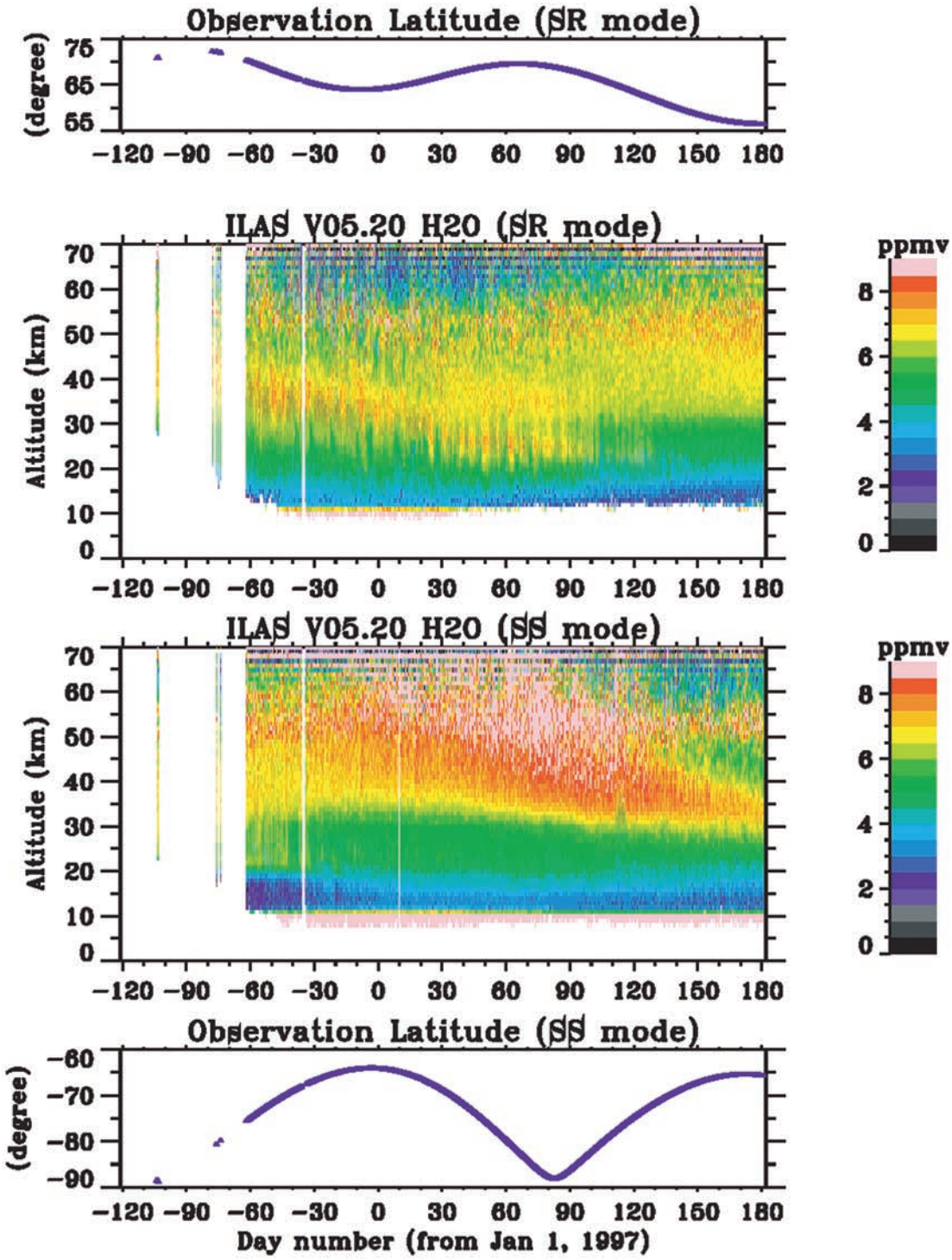

Figure 1. Time-altitude section of ILAS version 5.20 water vapor data from September 1996 to June 1997 using all available data in order of measurement time: Northern Hemisphere by sunrise (SR) occultation measurement (top panel) and Southern Hemisphere by sunset (SS) occultation measurement (bottom panel). Temporal changes of ILAS latitude coverage are also shown for each panel.

but we do not include it to the external error. We will evaluate the corresponding uncertainty later in this section.

[15] Effects from uncertainties in temperature, which are used in the calculation of simulated transmittance, are also included. These effects are evaluated imposing the uncertainties of ±2 K at 10 km altitude, ±5 K at 70 km altitude, and linear interpolation between these altitudes on a suitable model of temperature and gas profiles. The magnitudes of the external errors, defined as the root-sum-square (RSS) of these two errors due to the nongaseous component correction and the temperature profiles, were evaluated in advance to the routine data processing. The magnitudes of the

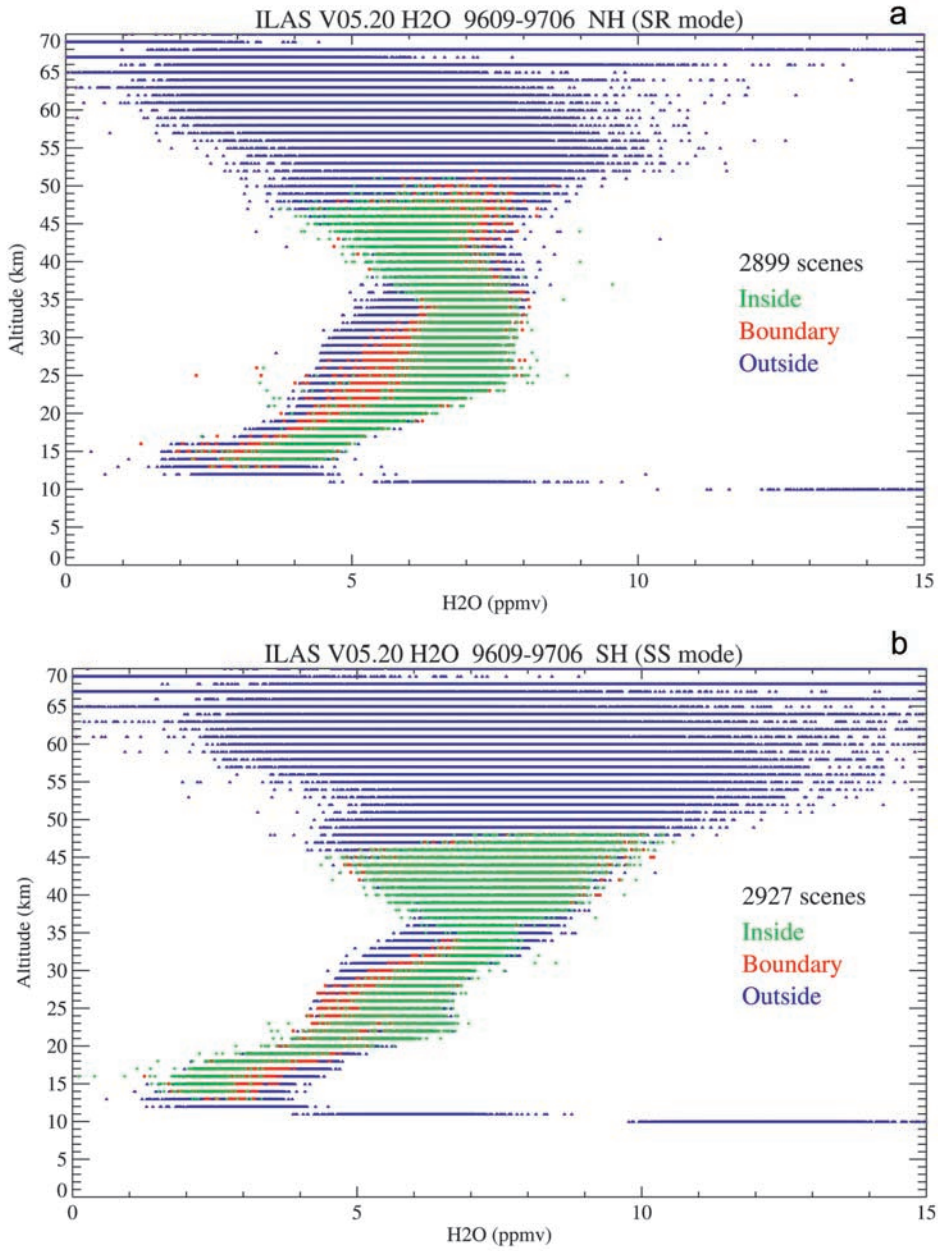

Figure 2. Vertical profiles of all available ILAS version 5.20 water vapor data for the Northern Hemisphere (a), and the Southern Hemisphere (b). Data are categorized into inside (green), boundary (red), and outside (dark blue) of the polar vortex.

external errors at each altitude were thus evaluated not for each measurement, but used in common for all water vapor data. A detailed description of the external error analysis is given by *Yokota et al.* [2002].

[16] In addition, the relative standard deviation (RSD) was calculated as the one-sigma standard deviation (around the mean) divided by the mean value over quiescent periods (3–5 days at the end of March 1997 in the SH or June 1997 in the NH). This quantity, RSD, includes a measure of geophysical variability and repeatability of the measurement. Since there was little geophysical variability in the quiescent periods, RSD is nearly equal to repeatability. RSD is thus considered as empirically determined precision because repeatability is a good measure of precision.

[17] Table 1 gives an overview of the errors. Using all version 5.20 water vapor data, we estimated average total errors (ppmv) in water vapor mixing ratio, and converted them into average percentage errors as detailed in the caption of Table 1. The average percentage error is 10%, 8%, 10%, 19%, 27%, and 39% at 15 km, 20 km, 30 km, 40 km, 50 km, and 60 km, respectively, as listed in Table 1. The relative standard deviation (RSD), a measure of precision, is 3%, 1%, 2%, 3%, 6%, and 12% at 15 km, 20 km, 30 km, 40 km, 50 km, and 60 km, respectively, as also listed

Table 1. Summary of Error Analysis for the ILAS Version 5.20 Water Vapor Data: Total Errors and Repeatability

Altitude, km	Average vmr,[a] ppmv	Internal Error,[b] ppmv	External Error,[c] ppmv	Total Error,[d] ppmv	RSD,[e] %	RSD,[e] ppmv	RSD,[e] ppmv
60	6.4	2.5	0.05	2.5	39	12	0.77
55	7.3	2.5	0.05	2.5	34	9	0.66
50	7.2	1.9	0.03	1.9	27	6	0.43
45	6.9	1.4	0.03	1.5	21	4	0.28
40	7.0	1.3	0.05	1.3	19	3	0.21
35	6.9	1.1	0.05	1.1	16	2	0.14
30	5.9	0.5	0.2	0.59	10	2	0.12
25	5.4	0.3	0.3	0.43	8	1	0.05
20	4.7	0.3	0.2	0.38	8	1	0.05
15	3.5	0.3	0.2	0.35	10	3	0.11
12	3.4	0.3	0.6	0.65	19	3	0.10
9	26.2	2.0	3.8	4.2	16	2	0.79

[a]Average volume mixing ratios (vmr) of all water vapor retrievals.
[b]Average of internal errors for all water vapor retrievals.
[c]External error, which is given in common for all water vapor data.
[d]Total error: RSS (root-sum-square) of internal and external errors (in ppmv) and its relative value (%). The latter is given by dividing the RSS by the average mixing ratio in the second column.
[e]Relative standard deviation (RSD in %), which is a measure of repeatability of the measurement, i.e. empirically determined precision (see text). For reference, the corresponding mixing ratio of RSD (in ppmv) is given by multiplying RSD (%) by the average volume mixing ratio in the second column.

in Table 1. The precision of ILAS water vapor measurements is excellent (less than 5%) below 45 km.

[18] Two points should be noted in terms of uncertainties in the retrieved profiles. First, accurate determination of the tangent height (TH) is crucial because TH ambiguity propagates to the uncertainty in retrieving volume mixing ratio profiles through the air density. The major difference between version 3.10, version 4.20, and version 5.20 profiles is due to how the Sun edge sensor measurements of ILAS have been used to determine TH: Version 3.10 did not use the Sun edge sensor measurements but relied on comparisons of measurements of the O_2 A-band (P-branch) transmittance in the ILAS visible channel with simulations based on UKMO (United Kingdom Meteorological Office) assimilated temperature and pressure data [*Swinbank and O'Neill*, 1994]. Version 4.20 used only the Sun edge sensor data. Version 5.20 uses both the Sun edge sensor data and the O_2 A-band data as described by *Nakajima et al.* [2002b]. The estimated systematic error in the altitude registration for the tangent point for version 5.20 is +300 ± 360 m: The errors of −60 m, +300 m, and +660 m as compared to the real TH correspond to errors of about +1%, −4%, and −9%, respectively, in volume mixing ratio of retrieved species including water vapor (Note that the estimated random error is 30 m). The TH error analyses are detailed also by *Nakajima et al.* [2002b]. For reference, the uncertainties in the altitude registration for SAGE II and HALOE are estimated to be 250 m and 150 m, respectively.

[19] The second point is systematic errors associated with the nongaseous component correction in the external error. To evaluate systematic errors caused by the simple linear interpolation between the window spectral elements, we simulated transmittances using several types of IR absorption spectra for sulfate aerosols of 50 and 75 wt% H_2SO_4/H_2O binary solutions and PSCs of nitric acid trihydrate (NAT), ice (ICE), and supercooled ternary solutions (STS) for four compositions as the nongaseous component and the reference profiles (a priori profiles) mentioned above as the gaseous component [*Yokota et al.*, 2002]. Using these simulated transmittances, retrievals of the vertical profile of the gaseous concentration were made after applying the linear interpolation method for the nongaseous contribution in the version 5.20 retrieval algorithm discussed here. The differences between a priori and retrieved water vapor profiles expressed in number density were well correlated with aerosol extinction coefficient (AEC) at 780 nm. Therefore the systematic errors in water vapor number density can be evaluated as a function of the AEC at 780 nm. Assuming typical air densities at altitudes of 15, 20, and 25 km, the errors in volume mixing ratios of water vapor ranged from −0.02 to −0.10 ppmv for the two types of sulfate aerosol with a value of the AEC of 5×10^{-4} km^{-1}, as listed in Table 2. These systematic biases for the several types of PSCs with a value of the AEC of 1×10^{-3} km^{-1} are also listed in Table 2. A detailed description of this error analysis is given by *Yokota et al.* [2002].

3. General Characteristics of ILAS Version 5.20 Water Vapor

[20] The internal consistency and general characteristics of the ILAS version 5.20 H_2O data are discussed in this section.

[21] Figure 1 shows time-altitude sections of H_2O using all available data in order of measurement time. The upper panel shows the section of the Northern Hemisphere (NH) sampled by the ILAS sunrise (SR) occultations with time variation of observation latitudes while the lower panel shows that of the Southern Hemisphere (SH) sampled by the ILAS sunset (SS) occultations. Continuous measurements from 30 October 1996 to 29 June 1997 are plotted as well as some test measurements on 17 and 18 of September and on 14, 16, 17, and 18 of October in 1996. The missing data on 25–26 November 1996 illustrated in white in Figure 1 result from the large number of sunspots during this period which make gas retrievals impossible. At the lowest altitude levels, the sunset occultation measurements in the SH extended a few km lower in altitude than the sunrise measurements in the NH because the Sun tracking for ILAS is easier at these lowest altitudes

Table 2. Summary of Error Analysis for the ILAS Version 5.20 Water Vapor Data: Systematic Biases (ppmv) Caused by the Nongaseous Component Correction[a]

Altitude, km	Sulfate Aerosols: AEC[b] = 0.0005 km^{-1}		Polar Stratospheric Clouds: AEC[b] = 0.001 km^{-1}					
	S(75)[c]	S(50)[c]	NAT	ICE	STS(5,37)[d]	STS(33,15)[d]	STS(47,3)[d]	STS(60,0.5)[d]
25	−0.10	−0.08	−3.84	−0.47	−1.52	0.01	0.15	−0.16
20	−0.05	−0.04	−1.73	−0.21	−0.69	0.01	0.07	−0.07
15	−0.02	−0.02	−0.79	−0.10	−0.31	0.00	0.03	−0.03

[a]See text for details.
[b]AEC: Aerosol extinction coefficient at 780 nm.
[c]S(75) and S(50) denote sulfate aerosols of 75 and 50wt%-H_2SO_4/H_2O binary solutions, respectively.
[d]STS(5,37), STS(33,15), STS(47,3), and STS(60,0.5) denote 5, 33, 47, and 60 wt%-H_2SO_4/37, 15, 3, and 0.5 wt%-HNO_3/H_2O supercooled ternary solutions of polar stratospheric clouds (PSCs), respectively.

in the sunset mode. Figure 1 indicates that the quality of the ILAS version 5.20 H_2O data is good in the following respects: (1) The value of mixing ratio, ranging from 3 to 8 ppmv, is reasonable within the uncertainties given in Tables 1 and 2 in section 2 (about 7 ppmv should be maximum); (2) The general feature of higher mixing ratios at higher altitudes is consistent with the production of water vapor from methane oxidation in the upper stratosphere and above; (3) Overall data look continuous in time and altitude with few abnormalities; (4) Typical features such as subsidence in the polar winter and dehydration in the Antarctic lower stratosphere are clearly visible. Figure 1 also indicates some poor quality data: (1) Data above about 55–60 km show unreasonable oscillation in altitude, most likely because any further smoothing is applied to this altitude region in spite of the low signal-to-noise ratio there; (2) Data at the lowest levels below around 12 km show little time variation; (3) Large values exceeding the anticipated maximum mixing ratio value of about 7 ppmv are sometimes seen especially in the SH. Poor quality data, especially the data above 55 km, should not be used for scientific analyses.

[22] Figure 2 shows vertical profiles of all available H_2O data for the NH (a) and the SH (b). The data are categorized as inside (green), boundary (red), and outside (dark blue) of the polar vortex on the basis of Ertel's potential vorticity (PV) gradient as a function of PV-based equivalent latitude [*Nash et al.*, 1996]. PV is calculated using the UKMO assimilation data [*Swinbank and O'Neill*, 1994], which were supplied as 24-hourly data at 12 UTC with resolutions of 2.5° in latitude and 3.75° in longitude, and at the UARS standard 22 pressure levels in the vertical from 1000 to 0.316 hPa (∼55 km) with a corresponding altitude resolution of about 2.5 km. For time periods and altitude ranges when the boundary of the polar vortex is not defined, the data are labeled as outside. In Figure 2, the outside data are plotted first, the boundary data second, and the inside data last: The inside data are thus most prominent in the figure.

[23] In the NH (Figure 2a), higher mixing ratios of water vapor are observed inside the polar vortex compared to those outside the vortex. This feature is consistent with our anticipation that water vapor is produced by oxidation of methane in the upper stratosphere and mesosphere and transported downward inside the polar vortex. In the SH (Figure 2b), the dehydration signal below about 27 km in the lower stratosphere from October to December 1996 masks this dynamical feature. Figures 2a and 2b show large values in the lowermost stratosphere around 10 km, minima around 13–15 km altitude, and a gradual increase up to around 40 km in both the Arctic and Antarctic. Above 40 km in the Arctic there is an overall decrease in water vapor mixing ratio with increasing altitude (Figure 2a) while in the Antarctic the opposite is true (Figure 2b). Furthermore, above 40 km in the Antarctic, there are many anomalous measurements of H_2O exceeding 10 ppmv. The unreasonable oscillation in mixing ratio with altitude above about 55–60 km shown in Figure 1 is reflected in Figure 2. The similar plots for each month (not shown) exhibit the following features: In general, the Arctic summer (June 1997) is similar to the Antarctic summer (December 1996), and the Arctic winter (December 1996) is similar to the Antarctic winter (June 1997). In other words, the profiles are symmetric in both polar regions with regard to season (with the exception of the dehydration signal in the Antarctic). The summer minimum feature around 15 km in the Antarctic is more prominent than that in the Arctic. The unreasonably high mixing ratios of over 10 ppmv (8 ppmv) above about 50 km (40 km) in the Antarctic are found prominently from February to April 1997. Most of the data in the Arctic are less than 8 ppmv except for high values due to the vertical oscillation above about 55 km.

4. Validation Experiments and Analysis Methods

[24] This section describes the methods used for validation of ILAS water vapor measurements using coincident validation measurements from other sources. The ILAS project organized a number of validation experiments [*Kanzawa et al.*, 1995; *Kanzawa*, 1997], including a balloon campaign at Esrange, near Kiruna, Sweden during the period from February to March 1997, which was the main field experiment [*Kanzawa et al.*, 1997]. A number of vertical profiles of water vapor as well as other gaseous species were obtained during that campaign. Another balloon campaign was carried out at Fort Wainright, near Fairbanks, Alaska [e.g., *Toon et al.*, 2002; *Jucks et al.*, 2002] in April–May 1997 and gave two reliable profiles of water vapor. ER-2 aircraft measurements of the POLARIS (Polar Ozone Loss in the Arctic Region in Summer) mission gave reliable water vapor data in April–May 1997. HALOE and SAGE II satellite sensors also measured water vapor during the ILAS measurement period.

Table 3. List of Coincidences of Water Vapor Validation Balloon Measurements and ILAS Measurements in 1997[a]

Balloon Instrument	Validation				ILAS				Difference	
	Date	Time	Latitude	Longitude	Date	Time	Latitude	Longitude	Time	Distance, km
FISH[b]	02/11	11:46	68.0	22.0	02/11	14:30	68.41	18.26	−02:44	161
LPMA[c]	02/14	14:40	65.80	22.80	02/14	13:08	68.69	41.31	01:32	853
ELHYSA[d]	02/14	21:44	67.81	23.92	02/14	13:08	68.69	41.31	08:36	719
LPMA[c]	02/26	15:30	66.90	20.50	02/26	14:26	69.49	33.76	01:04	616
MIPAS[e]	03/24	19:42	69.60	30.14	03/24	16:06	68.87	34.78	03:36	200
FIRS-2[f]	04/30	19:12	69.30	−148.91	04/30	06:04	63.57	−149.12	13:08	636
MkIV[g]	05/08	12:11	68.56	−146.29	05/08	05:49	62.14	−141.94	06:22	740

[a]The pairs of coincidence measurements are selected on the condition that the ILAS measurement is the nearest to the validation measurement in distance within 24 hours before and after the validation measurements in time. The time and location of validation measurements are described in the following footnote text, and those of ILAS measurements are the values at the tangent altitude of 20 km. The FISH, LPMA, ELHYSA, and MIPAS instruments were launched from Kiruna, Sweden (68°N, 21°E) and those of FIRS-2 and MkIV from Fairbanks, Alaska (65°N, 148°W). Dates and times of measurements are given in "MM/DD" and "hh:mm" in UTC in 1997, and locations of measurements are given in latitude degrees north and longitude degrees east ("-" means west). Differences of the time and location of ILAS measurement from those of validation measurement are given in "hh:mm" and in distance (km).
[b]time and position of FISH measurement at the altitude nearest to 20 km.
[c]Typical time and position of LPMA measurement.
[d]Time at the lowest altitude of ELHYSA measurement and the average position of the measurement.
[e]Averaged MIPAS time and position of tangent altitudes.
[f]Averaged time and position of FIRS-2 measurement.
[g]Time and position of MkIV measurement at 20 km altitude.

[25] Recently, a "Lagrangian approach" has been used to search for coincident measurement pairs using trajectory calculations. For example, *Morris et al.* [2000] suggested that results obtained using this approach are equivalent to, or improve upon, results obtained using the "traditional approach" of direct comparison of coincidence. Although the "Lagrangian approach" is capable of increasing the number of coincidence pairs with a little degradation of the comparison result, it is not expected to improve the results of this study for the following reasons: (1) The "Lagrangian approach" is a somewhat indirect comparison and is subject to error through its dependence on the quality of the meteorological data and the trajectory calculation method; (2) For satellite comparisons, enough events could be found using the "traditional approach", and comparisons were performed up to 70 km in altitude whereas above about 50 km no reliable meteorological data are available for the trajectory calculations; (3) Most of the ILAS validation balloon experiments were carried out sufficiently close in time and space to the corresponding ILAS measurements. We thus adopt the "traditional approach" of direct comparison of coincidence. It should be noted that the satellite and in situ data are responsive to different spatial scales, which may contribute to the observed differences between ILAS and the in situ comparison data sets.

[26] For validation studies, coincidence criteria with more relaxed longitude limits are often used by other groups. However, we did not use the relaxed longitude criteria for the following reasons: For comparisons at high latitudes, the polar vortex in winter-spring is often distorted with respect to the pole, causing longitudinal inhomogeneities in the tracer distribution. In the Northern Hemisphere (NH), the polar vortex formed in December 1996 and persisted exceptionally late, until early in May 1997 in the lower stratosphere, e.g., as seen from *NOAA* [2000a, Figure 8] and as described by *Coy et al.* [1997]. In the spring of 1996 in the Southern Hemisphere (SH), the polar vortex existed until the beginning of December 1996 in the lower stratosphere, e.g., as seen from *NOAA* [2000b, Figure 12]. PV analyses are incorporated to evaluate the degree of proximity of the comparison pairs in space in terms of dynamical conditions.

[27] In the following sections 5 to 7, we use the relative percentage difference of D defined as

$$D = [H_2O(ILAS) - H_2O(validation)]/\{[H_2O(ILAS) + H_2O(validation)]/2\} \times 100 \quad (1)$$

in percent (%) for each 1-km altitude grid, where "H_2O (ILAS)" and "H_2O (validation)" denote water vapor mixing ratio values of "ILAS" and "validation" measurements, respectively. The primary product retrieved from ILAS is a vertical profile of mixing ratio as a function of geometric altitude, and conversions between geometric altitude and geopotential height are made to aid comparisons of ILAS with some of the correlative measurement data sets if required.

5. Comparison With Validation Balloon Campaign Data

[28] During the eight-month period of continuous operation of the ILAS instrument from November 1996 to June 1997, balloon validation experiments were conducted at two high-latitude sites: Kiruna, Sweden (68°N, 21°E) and Fairbanks, Alaska (65°N, 148°W). For the validation of ILAS water vapor, seven flights of balloonborne instruments were made from February to May 1997 using six different techniques. These comparisons are listed in Table 3. The five measurements at Kiruna in February and March 1997 were made inside the polar vortex or close to its edge while the two measurements at Fairbanks in April and May 1997 were made outside the polar vortex.

[29] FISH (Fast In-situ Stratospheric Hygrometer) and ELHYSA (Etude de l'Hygrometrie Stratospherique et des Aerosols) are in situ measurement instruments. FISH is a Lyman-alpha fluorescence hygrometer [*Zöger et al.*, 1999a, 1999b] and ELHYSA is a frost point hygrometer [*Ovarlez*, 1991; *Ovarlez and Ovarlez*, 1994]. Others are remote sensing spectrometers. LPMA (Limb Profile Monitor of the Atmosphere) and MkIV are solar occultation FTIR (Fourier transform infrared) spectrometers. Details of the LPMA instrument are provided by *Camy-Peyret et al.*

[1995] and *Camy-Peyret* [1995], and those of MkIV by *Toon* [1991]. For LPMA, the occultation mode data are used here among the occultation and ascent modes of measurement. MIPAS (Michelson Interferometer for Passive Atmospheric Sounding) and FIRS (Far-Infrared Spectrometer)-2 are limb emission sounding spectrometers. Details of the MIPAS instrument and its data evaluation are described by *Fischer and Oelhaf* [1996] and *Friedl-Vallon et al.* [1999], and especially for water vapor retrieval by *Stowasser et al.* [1999], and those of FIRS-2 are given by *Johnson et al.* [1995] and *Jucks et al.* [1998]. These are well characterized and proven instruments, and with the exception of LPMA, they are reviewed and compared in detail in the SPARC Water Vapour Assessment [*Kley et al.*, 2000].

[30] Figure 3 shows vertical profiles of H_2O volume mixing ratio from ILAS and balloon validation measurements (left panel), relative percentage difference between ILAS and validation measurement with positive values denoting ILAS values higher than those of the validation measurement (central panel), and PV profiles at the locations of ILAS and validation measurements by relative percentage differences (right panel). The times and locations of the coincident pairs are given in Table 3 together with their determination method. The error bars for ILAS in Figure 3 (left panel) are the total errors defined in section 2. As for the error bars for the validation measurements, we classify the measurements into two types, remote sounding measurements and in situ measurements. One-sigma precision error bars were plotted for the remote sounding measurements of LPMA, MIPAS, FIRS-2, and MkIV. We do not draw error bars for the in situ measurements of FISH and ELHYSA, and just give information on the precision (random error) and accuracy (systematic error plus random error) in the caption. Here the relative percentage differences of water vapor (central panel) are defined as D in equation (1) by setting "validation" to be each balloon validation measurement. LPMA, FIRS-2, and MkIV data are given at the 1-km altitude grid. To extract data onto the 1-km altitude grid, MIPAS data are linearly interpolated, and FISH and ELHYSA data with fine vertical resolution are 1-km averaged in altitude. The relative PV percentage difference of DPV (right panel) is defined as

$$\mathrm{DPV} = [\mathrm{PV(X)} - \mathrm{PV(Y)}]/\mathrm{PV(Y)} \times 100 \qquad (2)$$

in percent (%) for each 1-km altitude grid, where "PV (X)" and "PV (Y)" denote PV values at the time and location of X and Y. We first specify X as "ILAS" and Y as "validation" in equation (2) to define an index of difference in air masses sampled. We use the horizontal positions and times of "ILAS" and "validation" given in Table 3, and interpolate PV values bilinearly in horizontal and linearly in time. We also define indices of the relative position with respect to the polar vortex edge by specifying X as "ILAS" and Y as "edge", and by specifying X as "validation" and Y as "edge", where "PV (edge)" is the PV at the polar vortex edge defined by *Nash et al.* [1996]. We use the times of "ILAS" and "validation" given in Table 3, and interpolate PV edge values linearly in time.

[31] The first set of five balloon validation experiments was carried out at Kiruna, Sweden in February and March 1997 mostly inside the polar vortex (Figures 3a–3e). On 11 February 1997, the Lyman-alpha hygrometer of FISH obtained data very close to an ILAS measurement with the difference in mixing ratio of less than 20% (Figure 3a). At 16–23 km the difference was −2 to +16%, increasing with altitude. The PV differences between the two measurement locations are very small, with the PV values at the location of ILAS measurement only slightly larger than that of FISH measurement above about 18 km, and both measurements were done inside the polar vortex because the PV difference values of "ILAS − Edge" and "Val − Edge" are both positive in the right panel.

[32] A few days later on 14 February, the balloon solar occultation measurement of LPMA (Figure 3b) showed that large percentage differences between ILAS and LPMA H_2O correspond to large PV differences: The ILAS location was inside the vortex whereas the LPMA location was near the vortex edge. It should be noted that the vertical profile of the percentage difference between ILAS and LPMA is very similar in shape to that of the PV difference in a reasonable way: Higher mixing ratios of water vapor correspond to higher values of PV, i.e., further inside the polar vortex.

[33] On the same day on 14 February, the frost point measurement of ELHYSA was available from about 21.5 to 28 km (Figure 3c). At the highest altitude, the difference is about 10%, but for the lower altitudes ILAS data are up to about 29% higher than those of ELHYSA. The vertical profile of the percentage difference of ILAS from ELHYSA is again very similar to that of the PV difference with a maximum of about 45%. The percentage difference of PV with respect to the vortex edge indicates that the location of ILAS measurement is further inside the vortex than ELHYSA, which partly explains the higher mixing ratio of water vapor in ILAS than in ELHYSA. At around 27–28 km, the location of ELHYSA is sufficiently inside the vortex, which reasonably explains the smaller difference in H_2O.

[34] Another comparison of ILAS with LPMA on 26 February (Figure 3d) shows good agreement with an exception at around 25–27 km, where LPMA shows extremely large values over 8 ppmv. Another exception is found at ~15 km, where the ILAS H_2O values are 21% larger than the LPMA. Some problems are suggested in the LPMA considering large error bars at the altitudes as shown in the figure. The measurement locations for both were very similar in terms of PV.

[35] A comparison of ILAS with the remote sensing emission measurements by MIPAS on 24 March (Figure 3e) shows that ILAS compares very well with MIPAS above 19 km, and is only 7% larger than MIPAS around 24–26 km. Below 19 km, ILAS gives smaller H_2O values. ILAS gives −38% difference at the lowest altitude of 13 km even though the PV difference is very small at these altitudes. The altitude profile of the differences is very similar to that found in the ILAS-FISH comparison. The difference at the lowest altitude may be due to poor retrieval of ILAS.

[36] In general, these high-latitude winter measurements might be affected by atmospheric variability. The variability of water vapor abundance near the vortex edge is a reasonable explanation for the observed altitude-dependent differences between the measurements. However, in general, the H_2O differences are partly due to the difference of

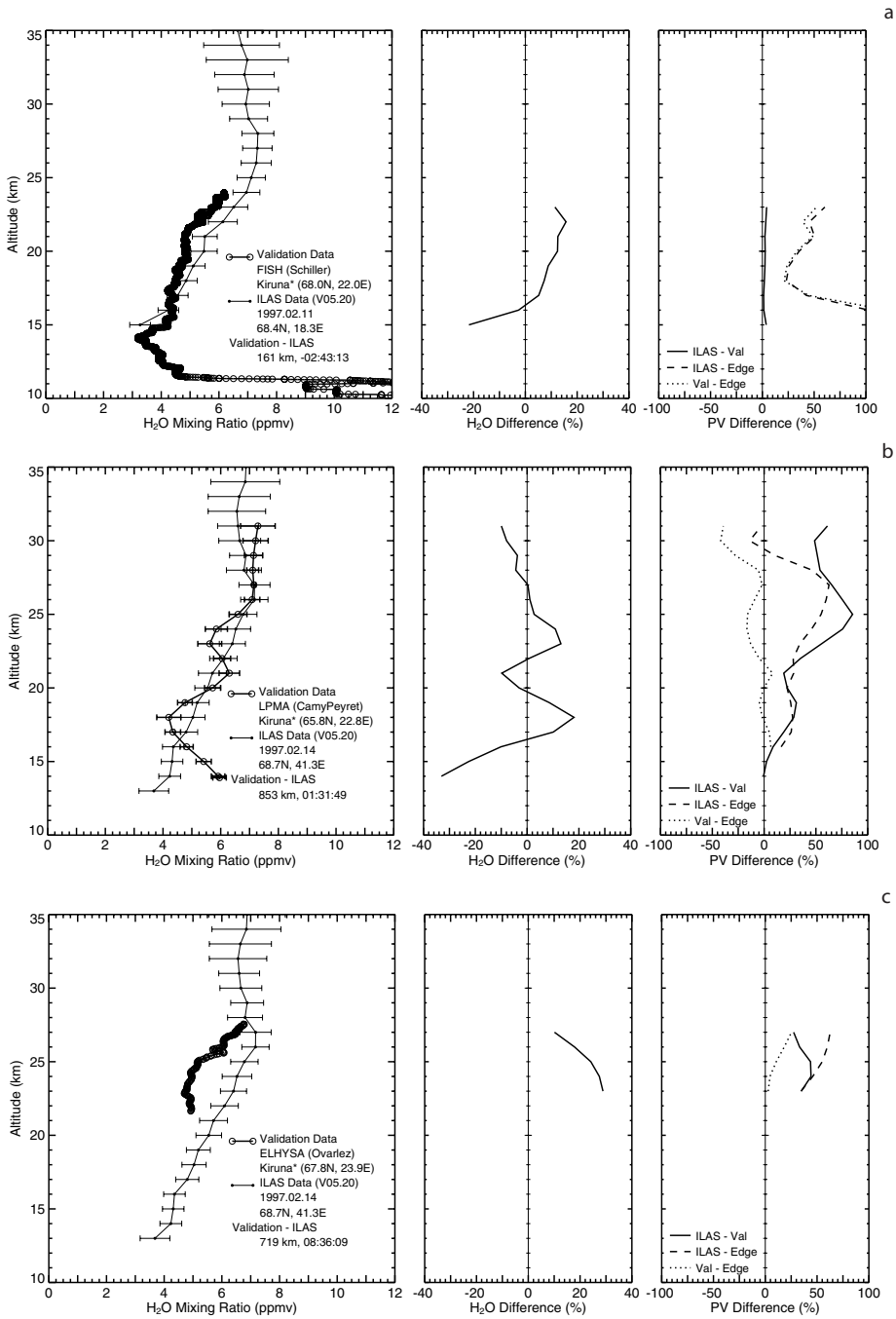

Figure 3. Comparison of vertical profiles of water vapor volume mixing ratio of ILAS version 5.20 measurement and balloon validation measurement, and relative percentage difference D (see section 4 for the definition), for the seven ILAS validation flights detailed in Table 3. The error bar of ILAS shows the total error defined in the text. The meanings of the error bars in the validation measurements are given in parentheses: (a) FISH (the error bars are not shown; 0.15 ppmv precision; 0.35 ppmv or 6% accuracy); (b) LPMA (one-sigma precision); (c) ELHYSA (the error bars are not shown; 3% precision: 6% accuracy); (d) LPMA (one-sigma precision); (e) MIPAS (one-sigma precision); (f) FIRS-2 (one-sigma precision); (g) MkIV (one-sigma precision). The vertical range of (a)–(e) is 10–35 km while that of (f)–(g) is 10–40 km. Comparison of Ertel's potential vorticity (PV) profiles at the locations of ILAS and validation measurements by percentage are added to the right-hand side of each panel (see section 5 for the definitions): Note that the lines of "ILAS edge" and "Val edge" are not drawn for the altitudes where the polar vortex edge cannot be defined as in the case of (f) and (g).

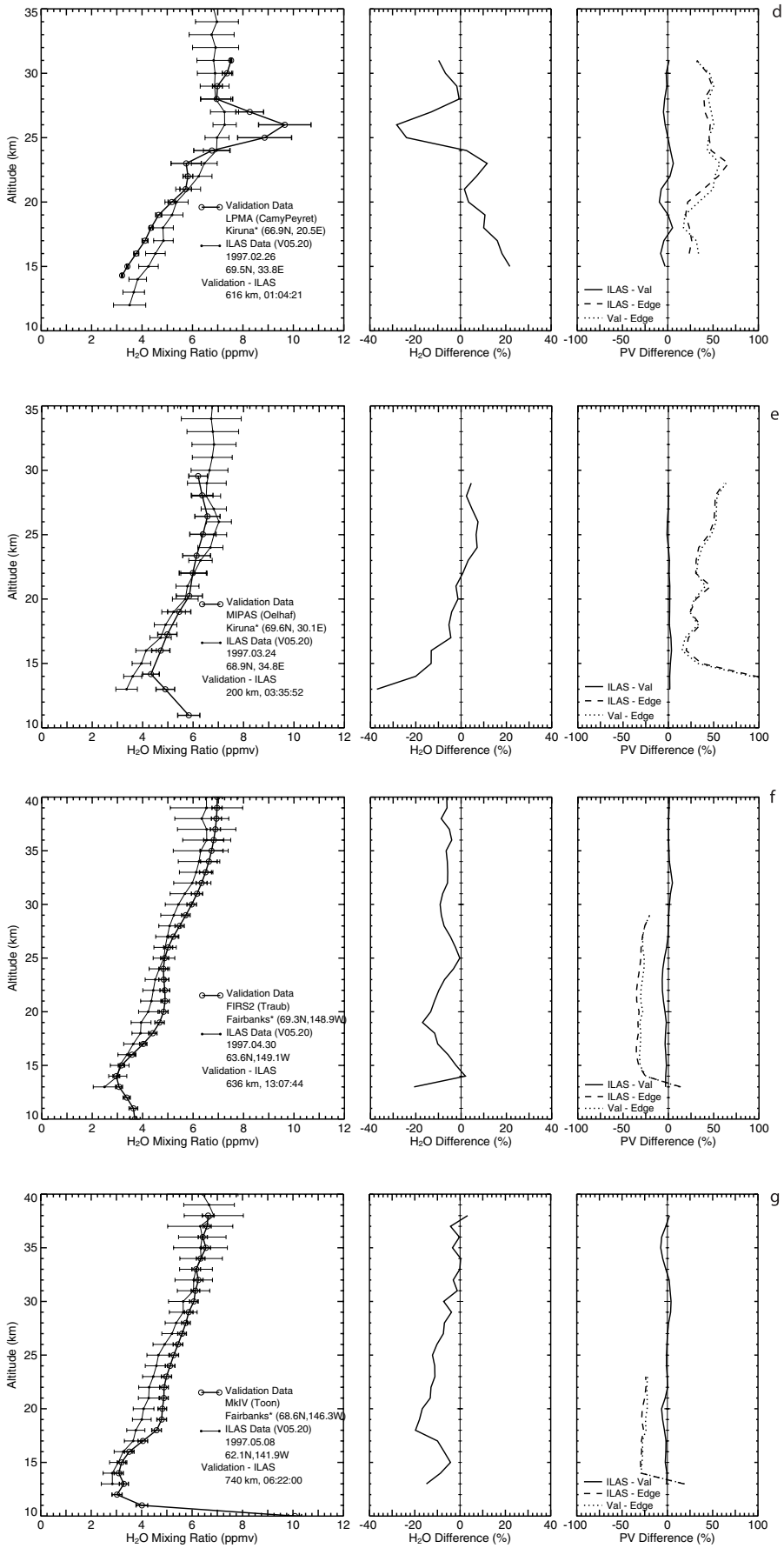

Figure 3. (continued)

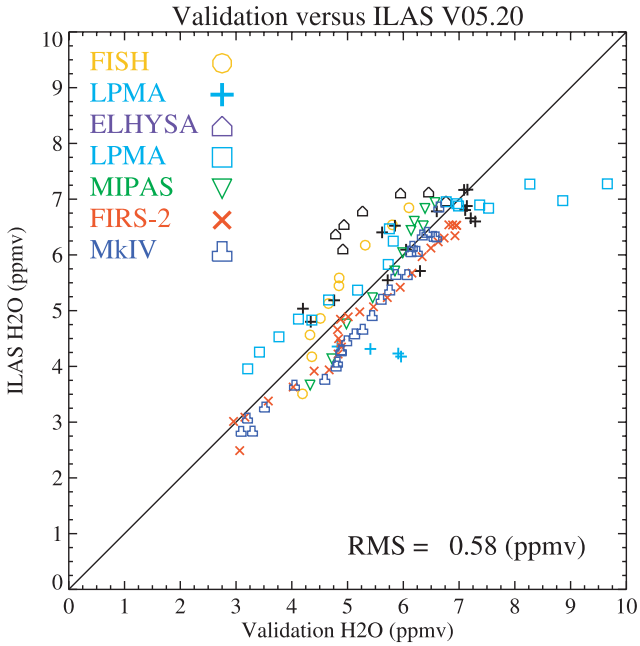

Figure 4. Correlation of ILAS version 5.20 water vapor versus balloon water vapor for all available coincidences. The black-colored marks show the pairs whose relative PV percentage differences are larger than 15%. Root-mean square (RMS) difference of ILAS data against balloon data (excluding the black-colored pairs) is shown to be 0.58 ppmv.

the measurement location with respect to the polar vortex edge as suggested in the right panel of each figure.

[37] The second set of two balloon validation experiments was carried out at Fairbanks, Alaska in April and May 1997 outside the polar vortex (Figures 3f–3g). On 30 April, the FIRS-2 emission spectrometer was flown up to an altitude of 40 km (Figure 3f). The relative percentage difference between ILAS and FIRS-2 data for 22–40 km and for 14–18 km was found to be −10% to 0% while that for 19–21 km was −17% to −10%. At the lowest altitude of 13 km, ILAS gives −20%. The validation flight on 8 May of the MkIV solar occultation spectrometer yields differences between −10% and +0% for the 14–17 km and 23–38 km altitude regions (Figure 3g). The difference for 18–22 km is −20% to −10% and the difference at 13 km is −14%. Although both the MkIV and FIRS-2 measurements give larger mixing ratios than those of ILAS, the differences do not indicate clear altitude dependence.

[38] Both balloon observations at Fairbanks, as well as the corresponding ILAS measurements, were made in air masses that were not much influenced by the vortex, which was still lingering over Northern Europe and Russia in early May 1997 [*Toon et al.*, 1999]. This is suggested by the fact that the PV percentage differences are small in Figures 3f and 3g. Further, the viewing geometry of both instruments was similar to that of ILAS. Thus, the conditions at Fairbanks were more favorable for comparison than those at Kiruna. This may explain why smaller differences were seen for the validation measurements by FIRS-2 and MkIV than those by FISH, ELHYSA, LPMA, and MIPAS.

[39] To summarize, Figure 4 shows a correlation scatterplot of ILAS version 5.20 H_2O versus balloon H_2O measurements for all available coincidences. The scatterplot confirms the good agreement of ILAS with balloon measurements as described above. Large differences between ILAS and LPMA are due mainly to differences in location relative to the polar vortex edge, and also because the quality of LPMA H_2O data is not as good as that of other species of LPMA because the spectral interval of LPMA is not optimal for H_2O. The higher bias of ILAS versus ELHYSA is mainly due to the difference in location relative to the polar vortex edge as described above. For reference, averages of the relative percentage differences (D) at selected altitudes for selected sample pairs in parentheses are as follows: −13% at 15 km (5 samples: FISH, LPMA, MIPAS, FIRS-2, MkIV), −5% at 20 km (4 samples: FISH, MIPAS, FIRS-2, MkIV), −6% at 25 km (2 samples: FIRS-2, MkIV), and −8% at 30 km (2 samples: FIRS-2, MkIV), as also given as a measure of accuracy of ILAS measurements by *Yokota et al.* [2002, Table 1]. Making allowance for steep spatial gradients in H_2O concentrations near the edge of the polar vortex, it can be concluded that the ILAS water vapor measurements in the 15–40 km altitude range fall within about 10% of the correlative measurements and within a root-mean square error of about 0.58 ppmv (given in Figure 4) from a variety of techniques of balloonborne instruments.

6. Comparison With Simultaneous ER-2 Aircraft Measurements From the POLARIS Mission

[40] In order to study photochemical and transport processes that cause the summer polar decreases in stratospheric ozone, the POLARIS (Photochemistry of Ozone Loss in the Arctic Region in Summer) mission was conducted in April–September 1997 [*Newman et al.*, 1999]. There were two instruments that measure H_2O on board the NASA ER-2 aircraft, which was deployed during the POLARIS mission. One is a Lyman-alpha hygrometer developed at Harvard University [e.g., *Weinstock et al.*, 1994], and the other is an open path, multipass Herriot cell, and a tunable infrared laser source (1.37 μm) absorption hygrometer developed at NASA/JPL (Jet Propulsion Laboratory) [e.g., *May*, 1998]. Measurement precision is estimated to be 0.05 ppmv in the stratosphere for a 2-s integration period. Comparisons of the JPL laser hygrometer with the Harvard Lyman-alpha hygrometer have shown the agreement to be better than 1% above 490 K potential temperature (∼19 km) during the June/July deployment [*Hintsa et al.*, 1999]. Near the hygropause, however, the JPL hygrometer measured H_2O values some 5–10% larger than the Harvard hygrometer.

[41] Table 4 summarizes the ILAS-POLARIS coincidences from the end of April to the middle of May 1997 during the first deployment period of the POLARIS ER-2 mission, which was based at Fairbanks, Alaska. In the third column of Table 4, HW represents the Harvard Lyman-alpha hygrometer, while JW represents the JPL laser hygrometer. A total of 10 H_2O profiles of POLARIS ER-2 were found whose minimum distance to the ILAS occultation tangent point was less than 500 km and whose time difference was within ±12 hours. The POLARIS ER-2 measurements as

Table 4. List of Coincidences of Validation Measurements of Two POLARIS Instruments and ILAS Measurements in 1997[a]

Profile	Month/Day	Instrument	Altitude Range	Minimum Distance
1	04/26	HW, JW	13–19 km	268.4 km
2	04/30	HW, JW	13–19 km	137.7 km
3	04/30	HW, JW	13–20 km	392.8 km
5	05/06	HW, JW	14–20 km	293.8 km
6	05/09	HW	13–19 km	367.1 km
7	05/09	HW, JW	13–19 km	431.9 km
8	05/11	HW, JW	13–19 km	425.7 km
9	05/11	HW, JW	13–19 km	392.7 km
10	05/13	JW	12–19 km	495.5 km

[a]The coincidence condition is that POLARIS ER-2 profiles whose minimum distance from the ILAS occultation tangent point is less than 500 km within ±12 hours time difference. HW represents the Harvard Lyman-α hygrometer, while JW represents the JPL laser hygrometer. The altitude of the comparison and its minimum distance are also shown.

well as the corresponding ILAS measurements were made in air masses that were not influenced by the polar vortex, which was still lingering over Northern Europe and Russia in early May 1997 as also noted in section 5. The altitude range of the comparison is also shown in Table 4.

[42] Figure 5 shows comparisons of ILAS version 5.20 H_2O and POLARIS aircraft validation measurements (left panel) with relative percentage differences (right panel). Here the relative percentage differences are defined as D in equation (1) by setting "validation" to be "POLARIS". The left panel of Figure 5 shows the averaged vertical profiles of ILAS and POLARIS (average of HW and JW) with their one standard deviation, and their minimum and maximum values. The figure shows that POLARIS gives higher mixing ratio values at all altitudes below 20 km compared with ILAS although the vertical gradient is almost the same. The mixing ratio differences seem to be significant since they exceed the standard deviations of those measurements. The relative percentage differences, plotted in the right panel of Figure 5, are about −27% to −16% for 14–20 km. Chapter 2 of the WAVAS report by *Kley et al.* [2000] showed that in the 100–60 hPa layer (about 16–19 km), HW is about 20% larger than HALOE, JW is about 1% larger than HW, and ILAS is about 3% larger than HALOE, which means that ILAS is about 17–18% smaller than HW and JW. This bias is consistent with the comparison of ILAS with HW and JW of POLARIS as shown in Figure 5. The magnitude of the percentage difference of 16–27% is, however, larger than that of the bias of 17–18%. The POLARIS ER-2 aircraft data thus support qualitatively the feature of smaller values of ILAS below 20 km that we found in the comparison of ILAS with two balloon measurements of FIRS-2 on 30 April 1997 and MkIV on 8 May 1997 launched from Fairbanks, Alaska, which were partly carried out as the POLARIS balloon mission.

7. Comparison With Simultaneous Satellite Measurements of HALOE and SAGE II

[43] In this section, ILAS version 5.20 water vapor is compared with HALOE version 19 water vapor and with SAGE II version 6 water vapor for the entire ILAS continuous measurement period between November 1996 and June 1997. All of the HALOE and SAGE II data are available for scientific use through their World Wide Web servers. To extract the coincidence pairs between ILAS and HALOE, and those between ILAS and SAGE II, we used criteria in time and space differences of ±12 hours and 300 km, respectively. For searching coincidence measurements, location and time at the tangent height of 20 km were used as being representative of each measurement. HALOE and

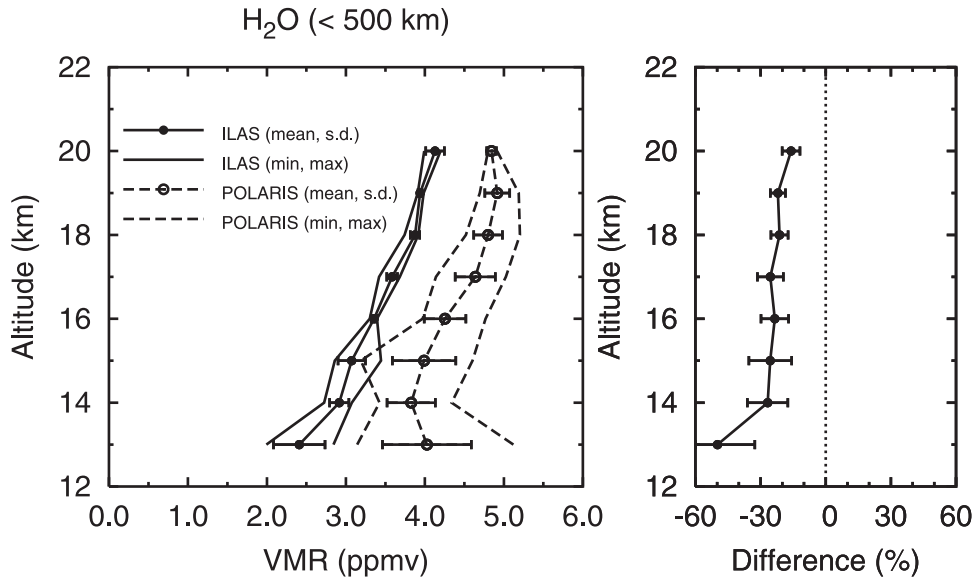

Figure 5. Comparison of vertical profiles of water vapor volume mixing ratio of ILAS version 5.20 measurements and POLARIS aircraft validation measurements using all coincidence pairs shown in Table 4. In the left panel, mean profile, its one-sigma standard deviation variance of each altitude, and minimum and maximum values are plotted for both ILAS and POLARIS. In the right panel, relative percentage difference (see section 4 for the definition) and its one-sigma standard deviation are shown.

Table 5. Summary of Water Vapor Coincidence Measurements of ILAS Versus HALOE and SAGE II for Each Period[a]

Period	Number	Distance, km[b]	Time, h[c]	Hemisphere[d]	Occultation Mode[e]	
					ILAS	Validation
HALOE Versus ILAS (*Total: 202; 118 in the SH and 84 in the NH*)[f]						
1996						
Nov 19–24	40	172 (28)	1.8 (3.5, 0.0)	SH	SS	SR
Dec 10–16	39	204 (130)	1.6 (3.5, 0.0)	SH	SS	SS
1997						
Jan 28–31	17	178 (19)	4.5 (5.3, 3.8)	SH	SS	SR
Feb 18–20	22	165 (64)	0.5 (1.0, 0.1)	SH	SS	SS
Mar 24–Apr 2	59	166 (23)	0.2 (0.5, 0.0)	NH	SR	SS
May 13–14	12	147 (9)	6.9 (7.4, 6.5)	NH	SR	SR
Jun 16–18	13	248 (197)	0.2 (0.4, 0.0)	NH	SR	SS
SAGE II Versus ILAS (*Total: 149*; *128 in the SH and 21 in the NH*)[f]						
1996						
Nov 4–24	74	149 (45)	1.4 (3.2, 0.0)	SH	SS	SR, SS
1997						
Jan 8–30	34	213 (136)	4.0 (4.8, 3.1)	SH	SS	SR, SS
Feb 3–4	20	194 (125)	0.5 (1.2, 0.0)	SH	SS	SS
Apr 26–29	10	188 (125)	7.9 (8.3, 7.4)	NH	SR	SR
May 28–30	11	220 (157)	0.2 (0.4, 0.0)	NH	SR	SS

[a]The coincidence pairs of measurements are selected on the conditions of maximum distance difference of 300 km and maximum time difference of 12 hours.
[b]Average of individual distances between observed locations. Minimum distance is shown in parentheses.
[c]Average of individual time difference between observation times. Maximum and minimum time differences are shown in parentheses, respectively.
[d]NH and SH represent solar occultation which occurred in the Northern Hemisphere and in the Southern Hemisphere, respectively.
[e]SR and SS represent sunrise and sunset, respectively, on the solar occultation events of each sensor.
[f]Numbers of coincidence measurements for each data set.

SAGE II are carried on inclined-orbit satellites so that the occultation events occur globally. Therefore coincidence latitudes are determined by the ILAS high latitude coverage ranging from 57° to 72° in the Northern Hemisphere (NH) and from 64° to 89° in the Southern Hemisphere (SH), depending on the season. With the criteria defined above, 202 coincidence pairs for HALOE versus ILAS and 149 coincidence pairs for SAGE II versus ILAS were selected in the first step. A summary of the coincidence measurements of satellite sensors is listed in Table 5, separately for periods shown in the table. The maximum time difference was 8.3 hours, which was found from the SAGE II versus ILAS pairs. Coincidences occurred in the SH during November 1996 to February 1997, and in the NH during March–June 1997. All ILAS NH measurements were obtained during satellite sunrise (SR), and all SH measurements during sunset (SS).

[44] Considering the relative position of the two measurements with respect to the polar vortex, the coincidence pairs selected by the above criteria were further screened by the following procedure. First, PV values at each tangent height location and time for ILAS and for its coincidence measurements were calculated. PV values and potential temperatures were calculated at each grid point. These data were then interpolated in time and space to each measurement (both for ILAS and its coincidence validation measurement) with 1-km geometric altitude grid. We defined the PV relative percentage difference as [PV (ILAS)−PV (validation)]/{[PV (ILAS) + PV (validation)]/2} × 100 in percent (%) for each 1-km altitude grid where PV (ILAS) and PV (validation) denote PV values at the time and location of ILAS and its coincidence validation measurement. If the relative percentage difference exceeds ±15% at consecutive altitude grids for more than 3 km, the data at these altitudes were discarded from the validation analysis.

[45] Figure 6a shows the results of all the ILAS-HALOE comparisons for 84 profiles of the Arctic during March–June 1997 and Figure 6b for 118 profiles of the Antarctic during November 1996 to February 1997. In the right panel, the median of individual percentage differences, D, between ILAS and HALOE is shown, together with its minimum and maximum. Here D is the relative percentage difference defined in equation (1) by setting ''validation'' to be ''HALOE''. Two dashed lines symmetrical with respect to the zero line show averages of RSS (root-sum-square) of the errors in the ILAS and HALOE measurements at each altitude, defined as the square root of the sum of total measurement errors of ILAS and HALOE data. The comparison for the Arctic spring and summer (Figure 6a) and the Antarctic late spring and summer (Figure 6b) shows, in general, fairly good agreement with differences of less than 10% at most altitudes. The Arctic comparison (Figure 6a) shows that the mean profiles of both ILAS and HALOE show a similar vertical structure in the lower stratosphere: Increasing mixing ratio with increasing altitude from 12 to 25 km (with ILAS about 0.5 ppmv smaller than HALOE), and almost constant from 25 to 32 km (with ILAS nearly equal to HALOE). From 32 to 60 km, although the profiles are still similar, ILAS has larger values by about 0.5–0.8 ppmv than HALOE. Above about 60 km, the ILAS mixing ratio has some unreasonable oscillation with altitude. The Antarctic comparison (Figure 6b) shows that the mean profiles of both ILAS and HALOE also show a similar vertical structure in the lower stratosphere: Decreasing

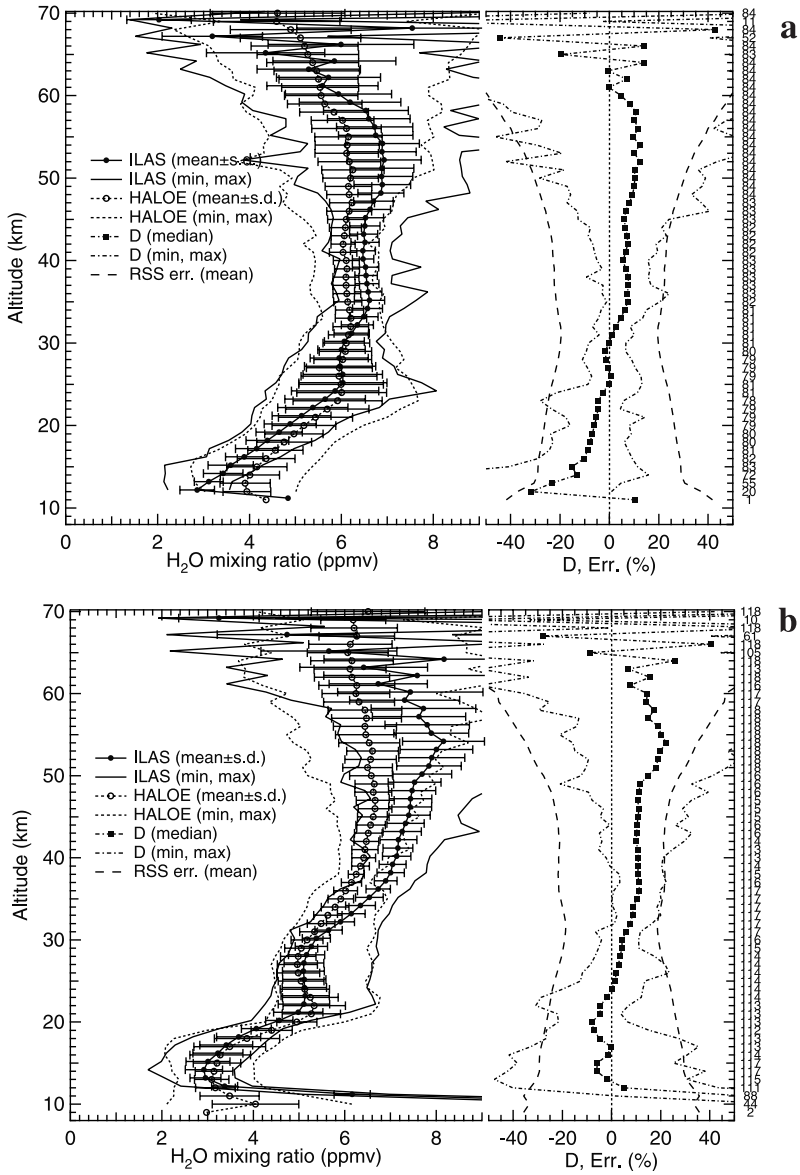

Figure 6. Water vapor comparison of ILAS with HALOE using all coincidence pairs shown in Table 5 for the Northern Hemisphere (a), and Southern Hemisphere (b). Average profiles of all coincident water vapor mixing ratios retrieved by ILAS version 5.20 and HALOE version 19 (left panel). The ILAS data are plotted with 0.2 km shift upward for clarity. Numbers of coincidence measurement pairs at each altitude are shown on the right-hand side of the figure. Bars show one-sigma standard deviation of the data at each altitude. Maximum and minimum of the data are shown as a solid line (ILAS) and a dotted line (HALOE), respectively. The median profile of individual relative percentage differences, labeled as D (see section 4 for the definition), between ILAS and HALOE water vapor mixing ratios is also shown (right panel). Maximum and minimum values of the data are shown as dash-dotted lines. Dashed lines symmetrical with respect to the zero line show the average of individual root-sum-square total uncertainties, labeled as RSS err., in ILAS and HALOE measurements (see text for the definition).

mixing ratio with increasing altitude from 12 to 15 km (with ILAS about 0.2 ppmv smaller than HALOE at the maximum difference), increasing mixing ratio with increasing altitude from 15 to 22 km (with ILAS about 0.3 ppmv smaller than HALOE), and almost constant from 22 to 30 km (with ILAS nearly equal to HALOE). From 30 to 55 km, increasing slope with altitude is sharper in ILAS than in HALOE (with ILAS about 1.6 ppmv larger than HALOE at the largest difference), giving about 8 ppmv mean mixing ratio for ILAS around 55 km. Above about 60 km, ILAS mixing ratio has also the unreasonable oscillation with altitude.

[46] Comparisons for the periods in each hemisphere with the maximum number of coincidences noted in Table 5 are shown in Figure 7a (24 March to 2 April, NH, 59 profiles) and Figure 7b (19–24 November 1996, SH, 40 profiles). During the Arctic early spring (Figure 7a), the vertical structure for both ILAS and HALOE measurements also

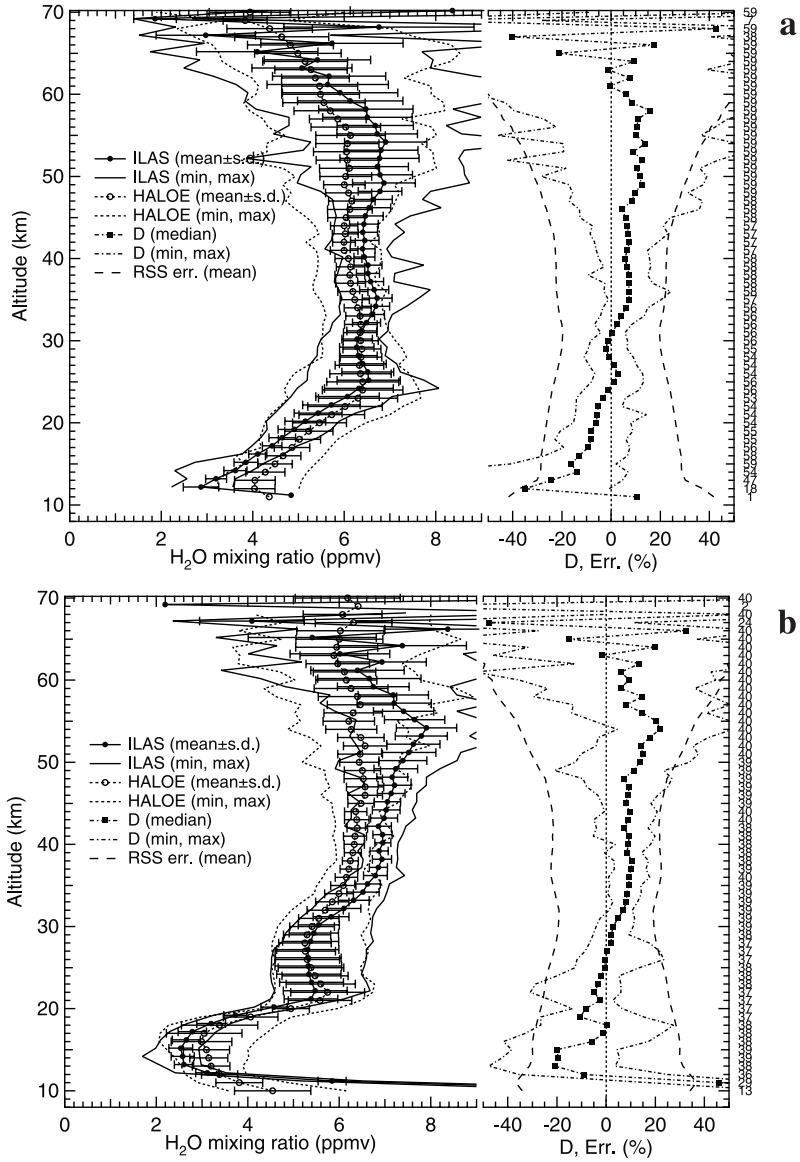

Figure 7. Same as in Figure 6 but for 59 comparisons of Northern Hemisphere measurements from 24 March to 2 April 1997 (a), and for 40 comparisons of Southern Hemisphere measurements from 19 to 24 November 1996 (b).

agrees well, with water vapor mixing ratio increasing with altitude up to about 25 km and then remaining nearly constant above that level up to about 55 km. Average differences throughout the bulk of the stratosphere are 10% or less except for the altitude below 15 km. The tendency of ILAS mixing ratios to be smaller than HALOE below about 25–30 km and larger above the altitude is similar to that of the comparison in the Antarctic November (Figure 7b) and December 1996. In the Arctic May 1997 (not shown), the vertical profiles of ILAS show a structure different from HALOE in the sense that HALOE shows a characteristic maximum around 23 km.

[47] The mean profiles of both ILAS and HALOE in the Antarctic late spring (Figure 7b) show a similar vertical structure, with minimum at ~15 km, maximum at ~22 km, and a secondary minimum at ~27 km. This is also seen in both instruments during the period of 10–16 December 1996 (not shown). ILAS gives smaller mixing ratios than HALOE below 25 km while larger mixing ratios than HALOE above 25 km. The right panel of Figure 7b shows that ILAS is about 10% lower than HALOE around 13–15 km while 20% higher around 55 km. High oscillation in the vertical direction is seen above around 65 km. At most altitudes except for these, the difference is smaller than 10% within the range of uncertainty of the measurements designated by RSS err. (mean) in the panel.

[48] In summary, comparison of ILAS version 5.20 with HALOE version 19 is very good considering the uncertainty of the measurements.

[49] Figure 8a shows the results of all the ILAS-SAGE II comparisons for 21 profiles of the Arctic during April–May 1997, and Figure 8b for 128 profiles of the Antarctic during November 1996 to February 1997. In the Arctic spring (Figure 8a), the mean profiles of both ILAS and SAGE II

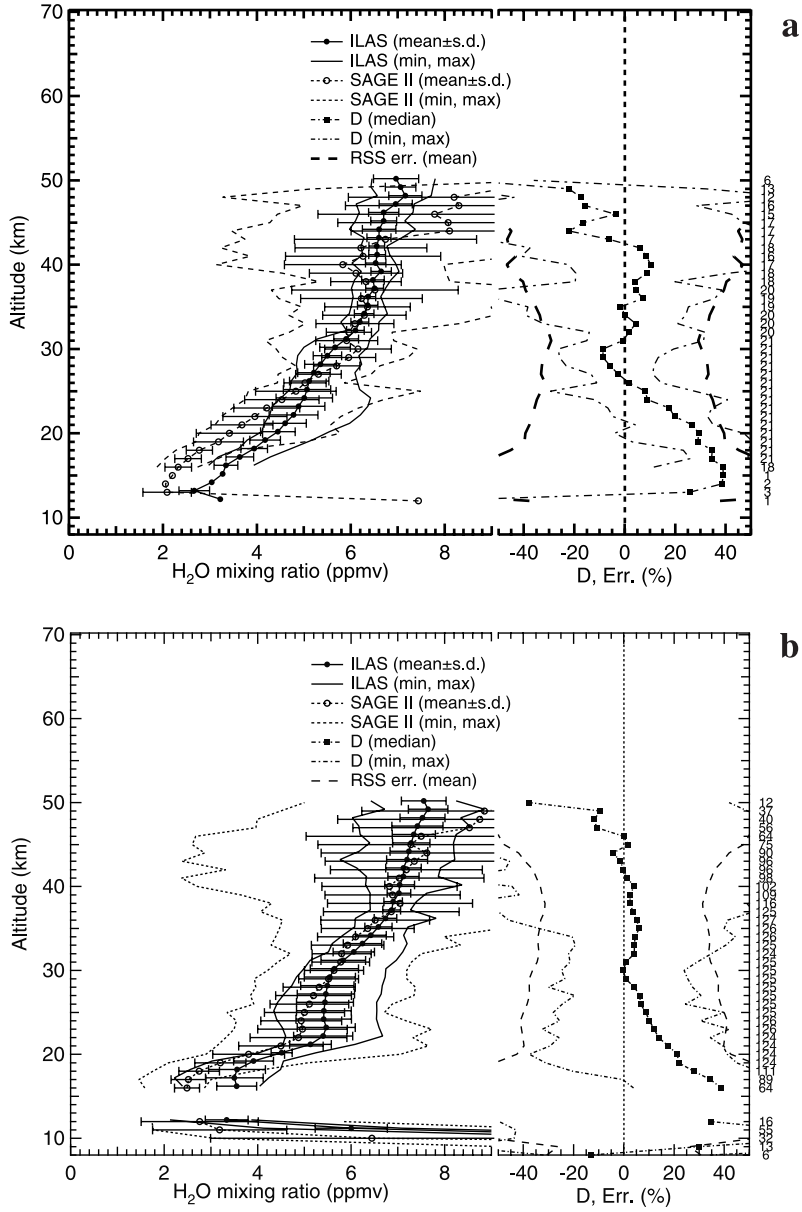

Figure 8. Same as in Figure 6 but for ILAS versus SAGE comparisons using all coincidence pairs shown in Table 5 for the Northern Hemisphere (a), and Southern Hemisphere (b).

show a rather monotonic increase with increasing altitude from 14 to 50 km and the slope is steeper in SAGE II profiles. SAGE II gives about 40% smaller values than ILAS at ~15 km. The difference is less than 10% for 25–43 km. In the Antarctic late spring and summer (Figure 8b), the mean profiles of both ILAS and SAGE II show a similar vertical structure, with minimum at ~17 km and maximum at ~23 km. Vertical profiles of the ILAS versus SAGE II percentage differences are similar to those of the Arctic spring.

8. Comparisons of Mean Variability in ILAS Data With HALOE and UARS Reference Atmosphere

[50] In addition to the comparisons with balloon- and aircraft- correlative measurements and satellite coincident measurements, comparisons of variability of monthly and zonal mean water vapor derived from ILAS with that in other satellite measurements are made as a part of validation analyses. This type of comparison, less quantitative by nature, is very useful in evaluating the data as a whole qualitatively. It assesses the consistency of ILAS measurements with the water vapor climatology established by other satellite measurements and with the known features of atmospheric circulation. In this section, we present a representative case of zonal mean comparisons with HALOE data and UARS climatology.

[51] Although the ILAS measurements were made at narrow latitude bands geographically (varying from 57°N to 72°N and from 64°S to 89°S), they covered a wide range of dynamic atmosphere due to steep PV gradients on potential temperature (theta) surfaces near the vortex edge and the distorted vortex shapes. When the measurements are

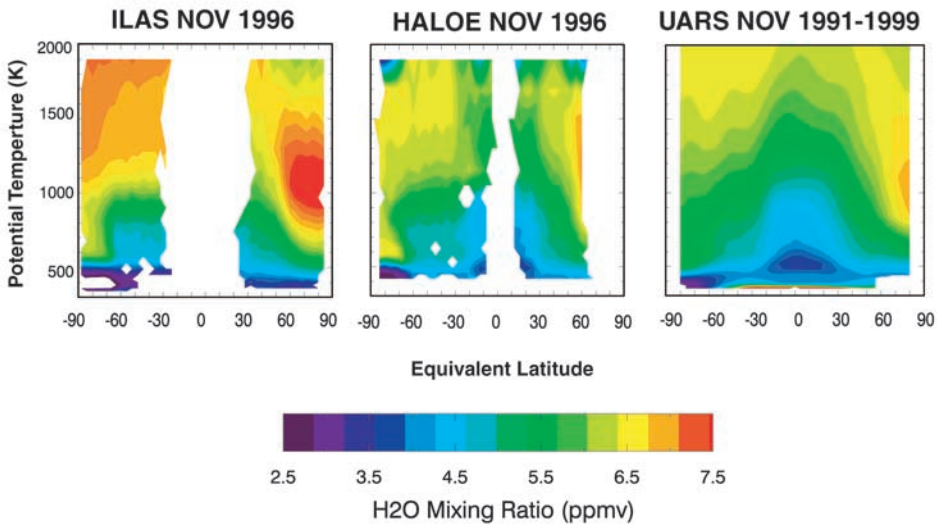

Figure 9. November water vapor monthly mean in PV-based equivalent latitude and potential temperature coordinates derived from ILAS 1996 measurements (left), HALOE 1996 measurements (center), and the UARS (9 years of 1991–1999) (right). Note the sampling range of HALOE instrument for this month was poleward limited to ~60°N in geographical latitude.

sorted by the dynamic variable PV, expressed as the PV-based equivalent latitude (EL) in this case, ILAS data covered approximately from about 30° to the pole in EL in both hemispheres.

[52] Figure 9 shows EL zonal means of ILAS and HALOE, both calculated from November 1996 measurements, and UARS climatology for November, calculated using nine years (1991–1999) of HALOE version 19 data and the 20 months of available MLS stratospheric water vapor prototype version 5 (nonlinear retrieval) data (9/1991–4/1993). The EL zonal means of ILAS and HALOE are binned averages using 4° latitude bands from 88°S to 88°N and the UARS standard theta levels. The PV and theta data are from the UKMO analyses. The UARS climatology is part of the UARS reference atmosphere and is derived from the seasonal cycle of binned averages in the same bands using a fit to seasonal harmonics of annual and semiannual [*Randel et al.*, 1998].

[53] Consistent with the UARS climatology, the ILAS EL zonal mean clearly shows that the ILAS data have captured features of the large-scale circulation in the stratosphere. Although the ILAS sampling did not cover the tropics in geographical latitude, the distributions indicate the ascent of air through the cold tropical tropopause and the edge of the polar vortices. The high values in the polar region indicate the descent of air with more water produced by methane oxidation. The dehydration signature in the Antarctic vortex of the lowermost stratosphere (below 500 K (~20 km) in Figure 9) during November, seen in the UARS climatology, is also represented in the ILAS climatology. The gradients in the water vapor distribution are remarkably similar in the ILAS and HALOE EL zonal means. The qualitative differences between the ILAS/HALOE 1996 zonal mean and the UARS nine-year climatology, e.g., the difference in gradients in the Southern Hemisphere (SH) 500–1000 K, reflect the interannual variability. The large visual difference between ILAS and HALOE EL zonal means in the Northern

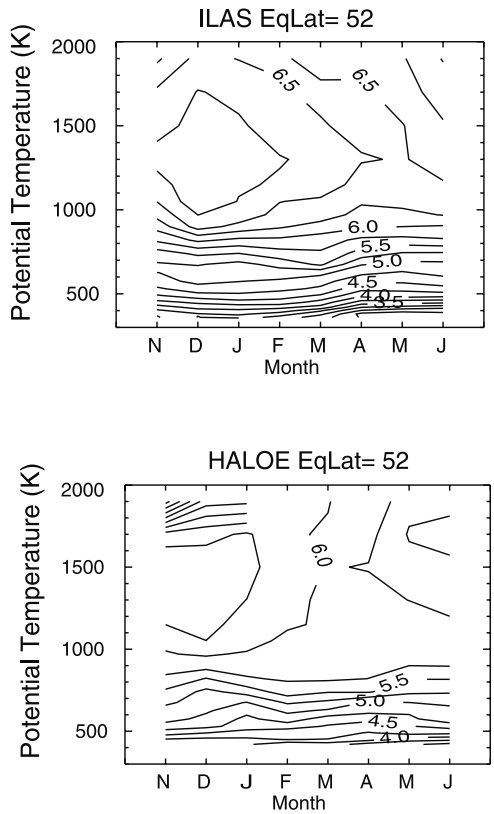

Figure 10. Time-height cross section of equivalent zonal mean of water vapor from November 1996 to June 1997 at 52°N PV-based equivalent latitude, derived from ILAS (top) and HALOE (bottom) measurements. The contours are in 0.25 ppmv intervals.

Table 6. Summary of Percentage Difference of ILAS Water Vapor Measurements Against Various Coincident Validation Measurements[a]

Altitude	1996				1997											
	Nov		Dec		Jan		Feb		Mar		Apr		May		Jun	
Experiment	NH	SH	NH	SH	NH	SH	NH	SH	NH	SH	NH	SH	NH	SH	NH	SH
50–60 km																
HALOE	*[b]	+10	*	+15	*	+15	*	+25	+10	*	*	*	+10	*	+5	*
45–50 km																
HALOE	*	+10	*	+10	*	+10	*	+15	+10	*	*	*	+5	*	+10	*
SAGE II	*	−10	*	*	*	−10	*	−10	*	*	−25	*	−10	*	*	*
40–45 km																
HALOE	*	+10	*	+10	*	+10	*	+15	+5	*	*	*	+5	*	+5	*
SAGE II	*	−5	*	*	*	−0	*	+0	*	*	+10	*	−10	*	*	*
35–40 km																
HALOE	*	+10	*	+10	*	+10	*	+15	+5	*	*	*	+10	*	+5	*
SAGE II	*	−0	*	*	*	+5	*	+10	*	*	+10	*	+5	*	*	*
BALLOON											−5FS		−0Mk			
30–35 km																
HALOE	*	+5	*	+5	*	+10	*	+10	+5	*	*	*	+5	*	+5	*
SAGE II	*	+0	*	*	*	+5	*	+5	*	*	0	*	−0	*	*	*
BALLOON											−5FS		−0Mk			
25–30 km																
HALOE	*	+0	*	+0	*	+5	*	+5	0	*	*	*	−5	*	0	*
SAGE II	*	+0	*	*	*	+10	*	+10	*	*	0	*	−5	*	*	*
BALLOON							−5LP +10EL −10LP		+5MI		−5FS		−5Mk			
20–25 km																
HALOE	*	−0	*	−5	*	−0	*	+0	−5	*	*	*	−5	*	−5	*
SAGE II	*	+5[c]	*	*	*	+20[c]	*	+20[c]	*	*	+20[c]	*	+15[c]	*	*	*
BALLOON							+15FI −+10LP +25EL +−10LP		+5MI		−5FS		−10Mk			
15–20 km																
HALOE	*	−5	*	−5	*	−5	*	−0	−10	*	*	*	−10	*	−5	*
SAGE II	*	+15[c]	*	*	*	+35[c]	*	+30[c]	*	*	+35[c]	*	+35[c]	*	*	*
POLARIS													−25			
BALLOON							−+10FI −+20LP +10LP		−5MI		−5FS		−10Mk			
10–15 km																
HALOE	*	−20	*	−5	*	+10	*	+5	−20	*	*	*	−10	*	−5	*
POLARIS													−30			
BALLOON									−20MI		−10FS		−10Mk			

[a]The table is arranged by altitude range, validation experiment, month, and hemisphere. NH and SH represent Northern Hemisphere and Southern Hemisphere, respectively. HALOE and SAGE II are satellite measurements. POLARIS consists of aircraft measurements. Balloon measurements include FISH (designated by FI), LPMA (LP), ELHYSA (EL), MIPAS (MI), FIRS-2 (FS), and MkIV (Mk). The percent figures are estimated with an interval of 5%. The positive values mean that ILAS is larger than validation. The notation "+−10" means that the values change within the altitude region with plus (+10) in lower altitudes and minus (−10) in higher altitudes, and vice versa. The notation "−0" means that the values are zero but slightly less than zero, and vice versa.

[b]The asterisk denotes no satellite measurements in the month and the hemisphere.

[c]The values change in the altitude region with plus (+) in lower altitudes and minus (−) in higher altitudes, and vice versa. The notation "−0" means the values are zero but slightly less than zero, and vice versa.

[d]The percent figures are not suitable for evaluation of ILAS (see text).

Hemisphere (NH) is largely due to the difference in the sampling range: In geographical latitude, ILAS sampled at around 70°N but HALOE is poleward limited to 60°N. Quantitatively, ILAS produced higher mixing ratio values than HALOE in the altitude region above 1000 K (∼35 km) and inside the polar vortex.

[54] The consistency of ILAS data with the large-scale circulation is also observed in the time-height cross section. Figure 10 displays water vapor EL zonal mean at 52°N EL from November 1996 to June 1997, derived from ILAS (top) and HALOE (bottom) measurements. Both ILAS and HALOE data show the seasonal variation in the NH middle stratosphere (above 800 K (∼30 km)) with the maximum in northern winter. The seasonal variation in this middle latitude EL band is a result of descent in the polar region. The difference between the ILAS and HALOE is largely due to the sampling difference of the two instruments. ILAS sampled mostly high latitude/polar air while HALOE zonal mean contains contributions from the low latitude air. The lower stratosphere water vapor is fairly constant in time in both data sets, but ILAS data show larger vertical gradients, consistent with the case comparisons shown in Figures 3 and 4.

[55] The overall consistency between the zonal mean climatologies shown in Figure 9 and Figure 10 is an important validation for the ILAS data as a whole. A more detailed discussion of zonal monthly variability of ILAS water vapor and its comparison with UARS clima-

tology is given by *Pan et al.* [2002], where the consistency between ILAS water vapor data and the meteorological conditions of the 1996/1997 Arctic vortex is further demonstrated.

9. Summary of Comparisons and Conclusions

[56] Table 6 summarizes the comparisons of ILAS measurements against various simultaneous validation measurements in sections 5, 6, and 7. The table is arranged by altitude range, validation experiment, month, and hemisphere. For 60–70 km, we do not show the comparisons because the ILAS profiles oscillate significantly in the vertical direction due to some problems in the retrieval. SAGE II satellite measurements have smaller values than ILAS measurements by more than 30% from 15 to 20 km and 20% from 20 to 25 km in the Antarctic summer of January and February 1997 and in the Arctic late spring of April and May 1997. As found by *Kley et al.* [2000], the quality of SAGE II especially for these altitude ranges is not sufficiently good because SAGE II values are much smaller than those of other experiments. An initial look at the summary of Table 6 shows that ILAS compares very well with all the available validation measurements, considering the uncertainty in the measurements of both ILAS and validation instruments. The climatological comparisons of ILAS with UARS climatology and HALOE data in the coordinates of PV-based equivalent latitude and potential temperature in section 8 show the overall consistency of ILAS water vapor data considering the known features of atmospheric circulation.

[57] ILAS data users should note that the ILAS version 5.20 water vapor data appear to have the following characteristics:

1. ILAS water vapor in the altitude region of 15–60 km is usually within 20% of all other reliable correlative measurements we compared, except for some cases as detailed in this paper, and is better than 10% for the majority of cases depending on altitude range, season, and hemisphere, as summarized in Table 6.

2. ILAS yields good quality as far as relative variation is concerned. The reliability of data regarding relative variation, however, depends on temporal and spatial scales concerned.

3. The quality of the ILAS measurements depends on season. For example, for 15–25 km in the Arctic, ILAS has a rather positive bias in February while a negative bias in May. For 10–25 km in the Antarctic, ILAS has a rather negative bias in November and December, while the negative bias is not so evident in February.

4. The quality of the ILAS measurements depends on altitude. For example, in the Arctic May 1997, ILAS has a rather negative bias below 30 km while a rather positive bias above 30 km. In the Antarctic November and December 1996, ILAS has a negative bias below 25 km while a rather positive bias above 25 km. ILAS in the Southern Hemisphere in January–April above about 40–50 km shows unreasonably high mixing ratios of water vapor over 8–10 ppmv.

[58] Summarizing the overall comparisons in this paper, the quality of ILAS version 5.20 water vapor was shown to be reasonably good for most scientific purposes such as studies on the polar stratospheric phenomena provided that the points shown in this paper are noted. The characteristics of ILAS measurements, i.e., high frequency measurements in high latitudes with high vertical resolution, and the reasonable quality of the ILAS water vapor measurements which are comparable to those of other satellite sensors such as HALOE, should prove useful to the stratospheric science community.

[59] **Acknowledgments.** Several ILAS science team members besides the authors made valuable contributions to discussions on validation issues. Constructive and detailed comments by two anonymous referees improved the paper. The Kiruna balloon campaign was realized by colleagues at EA (now MOE) headquarters (especially Katsuhiko Naito, Shinsuke Unisuga), CNES headquarters (especially Itziar Sadourny, Nicole Papineau), CNES balloon operation (especially Pierre Faucon), SSC/ESRANGE (especially J. Englund), and many other scientists and engineers. The Fairbanks balloon campaign was realized by many colleagues such as NASDA organizers (especially Toshihiro Ogawa, Kazuo Shibasaki), NASA organizers (especially Dean Peterson, Mike Kurylo), NSBF, and other scientists and engineers. The HALOE, SAGE II, POLARIS, and UARS Reference Atmosphere projects provided valuable data sets. The URL addresses of each WWW server of the respective projects as well as the ILAS project are as follows: HALOE, http://haloedata.larc.nasa.gov/; SAGE II, http://www-sage2.larc.nasa.gov/; POLARIS, http://cloud1.arc. nasa.gov/polaris/; UARS Reference Atmosphere, http://code916.gsfc.nasa.gov/Public/Analysis/UARS/urap/home.html; ILAS, http://www-ilas.nies.go.jp/. FUJITSU FIP engineers supported the analyses. ILAS data processing and most of the data analyses were carried out at the ILAS Data Handling Facility (DHF) at NIES.

References

Andrews, D. G., J. R. Holton, and C. B. Leovy, *Middle Atmosphere Dynamics*, 489 pp., Academic, San Diego, Calif., 1987.

Burton, S. P., L. W. Thomason, Y. Sasano, and S. Hayashida, Comparison of aerosol extinction measurements by ILAS and SAGE II, *Geophys. Res. Lett.*, *26*, 1719–1722, 1999.

Camy-Peyret, C., Balloon-borne Fourier transform spectroscopy for measurements of atmospheric trace gases, *Spectrochim. Acta*, *51A*, 1143–1152, 1995.

Camy-Peyret, C., P. Jeseck, T. Hawat, G. Durry, S. Payan, G. Berube, L. Rochette, and D. Huguenin, The LPMA balloon-borne FTIR spectrometer for remote sensing of atmospheric constituents, *ESA SP-370*, pp. 323–328, Eur. Space Agency, Paris, 1995.

Chiou, E. W., M. P. McCormick, and W. P. Chu, Global water vapor distribution in the stratosphere and upper troposphere derived from 5.5 years of SAGE II observations (1986–1991), *J. Geophys. Res.*, *102*, 19,105–19,118, 1997.

Coy, L., E. R. Nash, and P. A. Newman, Meteorology of the polar vortex: Spring 1997, *Geophys. Res. Lett.*, *24*, 2693–2696, 1997.

Fischer, H., and H. Oelhaf, Remote sensing of vertical profiles of atmospheric trace constituents with MIPAS limb-emission spectrometers, *Appl. Opt.*, *35*, 2787–2796, 1996.

Friedl-Vallon, F., G. Maucher, H. Oelhaf, M. Seefeldner, O. Trieschmann, G. Wetzel, and H. Fischer, The balloon-borne Michelson Interferometer for Passive Atmospheric Sounding (MIPAS-B2)—Instrument and results, *J. Soc. Photo-Opt. Instrum. Eng.*, *3756*, 9–16, 1999.

Gille, J. C., and J. M. Russell III, The limb infrared monitor of the stratosphere: Experiment description, performance, and results, *J. Geophys. Res.*, *89*, 5125–5140, 1984.

Harries, J. E., The greenhouse Earth: A view from space, *Q. J. R. Meteorol. Soc.*, *122*, 799–818, 1996.

Harries, J. E., J. M. Russell III, A. F. Tuck, L. L. Gordley, P. Purcell, K. Stone, R. M. Bevilacqua, M. Gunson, G. Nedoluha, and W. A. Traub, Validation of measurements of water vapor from the Halogen Occultation Experiment (HALOE), *J. Geophys. Res.*, *101*, 10,205–10,216, 1996.

Hayashida, S., N. Saitoh, A. Kagawa, T. Yokota, M. Suzuki, H. Nakajima, and Y. Sasano, Arctic polar stratospheric clouds observed with the Improved Limb Atmospheric Spectrometer during winter 1996/1997, *J. Geophys. Res.*, *105*, 24,715–24,730, 2000.

Hintsa, E. J., E. M. Weinstock, J. G. Anderson, R. D. May, and D. F. Hurst, On the accuracy of in situ water vapor measurements in the troposphere and lower stratosphere with the Harvard Lyman-α hygrometer, *J. Geophys. Res.*, *104*, 8183–8189, 1999.

Irie, H., et al., Validation of NO_2 and HNO_3 measurements from the Improved Limb Atmospheric Spectrometer (ILAS) with the version

5.20 retrieval algorithm, *J. Geophys. Res.*, *107*(D24), 8206, doi:10.1029/2001JD001304, 2002.

Johnson, D. G., K. W. Jucks, W. A. Traub, and K. V. Chance, Smithsonian stratospheric far-infrared spectrometer and data reduction system, *J. Geophys. Res.*, *100*, 3091–3106, 1995.

Jones, R. L., J. A. Pyle, J. E. Harries, A. M. Zavody, J. M. Russell III, and J. C. Gille, The water vapor budget of the stratosphere studied using LIMS and SAMS satellite data, *Q. J. R. Meteorol. Soc.*, *112*, 1127–1143, 1986.

Jucks, K. W., D. G. Johnson, K. V. Chance, W. A. Traub, J. J. Margitan, G. B. Osterman, R. J. Salawitch, and Y. Sasano, Observations of OH, HO_2, H_2O, and O_3 in the upper stratosphere: Implications for HO_x photochemistry, *Geophys. Res. Lett.*, *25*, 3935–3938, 1998.

Jucks, K. W., et al., Validation of ILAS v5.2 data with FIRS-2 balloon observations, *J. Geophys. Res.*, *107*(D21), 4566, doi:10.1029/2001JD000578, 2002.

Kanzawa, H., *ILAS and RIS Data Handling Facility USAGE GUIDE* (*Version 1*), *Rep. F-104-'97/NIES*, 70 pp., Nat. Inst. for Environ. Studies, Tsukuba, Japan, 1996.

Kanzawa, H., *ILAS Correlative Measurements Plan*, *Rep. F-105-'97-NIES*, 178 pp., Nat. Inst. for Environ. Studies, Tsukuba, Japan, 1997.

Kanzawa, H., Y. Kondo, C. Camy-Peyret, and Y. Sasano, Balloon campaigns at Kiruna-Esrange planned in ILAS Correlative Measurements Program, in *Proceedings of the 12th ESA Symposium on European Rocket and Balloon Programmes and Related Research*, *Lillehammer*, *Norway, 29 May to 1 June 1995*, pp. 345–349, Eur. Space Agency, Paris, 1995.

Kanzawa, H., C. Camy-Peyret, Y. Kondo, and N. Papineau, Implementation and first scientific results of the ILAS Validation Balloon Campaign at Kiruna-Esrange in February–March 1997, in *Proceedings of the 13th ESA Symposium on European Rocket and Balloon Programmes and Related Research*, *Oland, Sweden*, *26–29 May 1997*, pp. 211–215, Eur. Space Agency, Paris, 1997.

Kley, D., J. M. Russell III, and C. Phillips (Eds.), *SPARC Assessment of Upper Tropospheric and Stratospheric Water Vapour*, *WMO/TD Rep. 1043*, *SPARC Rep. 2*, World Meteorol. Org., Geneva, 2000. (Available at http://www.aero.jussieu.fr/~sparc).

Koike, M., et al., A comparison of Arctic HNO_3 profiles measured by the Improved Limb Atmospheric Spectrometer and balloonborne sensors, *J. Geophys. Res.*, *105*, 6761–6771, 2000.

Lahoz, W. A., et al., Validation of UARS Microwave Limb Sounder 183 GHz H_2O measurements, *J. Geophys. Res.*, *101*, 10,129–10,149, 1996.

Lee, K.-M., J. M. McInerney, Y. Sasano, J. H. Park, W. Choi, and J. M. Russell III, Intercomparison of ILAS and HALOE ozone at high latitudes, *Geophys. Res. Lett.*, *26*, 835–838, 1999.

Lucke, R. L., et al., The Polar Ozone and Aerosol Measurement (POAM III) instrument and early validation results, *J. Geophys. Res.*, *104*, 18,785–18,799, 1999.

May, R. D., Open-path, near-infrared tunable diode laser spectrometer for atmospheric measurements of H_2O, *J. Geophys. Res.*, *103*, 19,161–19,172, 1998.

McCormick, M. P., E. W. Chiou, L. R. McMaster, W. P. Chu, J. C. Larsen, D. Rind, and S. Oltmans, Annual variations of water vapor in the stratosphere and upper troposphere observed by the stratospheric aerosol and gas experiment II, *J. Geophys. Res.*, *98*, 4867–4874, 1993.

Morris, G. A., J. F. Gleason, J. Ziemke, and M. R. Schoeberl, Trajectory mapping: A tool for validation of trace gas observation, *J. Geophys. Res.*, *105*, 17,875–17,894, 2000.

Mote, P. W., K. H. Rosenlof, M. E. McIntyre, E. S. Carr, J. C. Gille, J. R. Holton, J. S. Kinnersley, H. C. Pumphrey, J. M. Russell III, and J. W. Waters, An atmospheric tape recorder: The imprint of tropical tropopause temperatures on stratospheric water vapor, *J. Geophys. Res.*, *101*, 3989–4006, 1996.

Nakajima, H., et al., Characteristics and performance of the Improved Limb Atmospheric Spectrometer (ILAS) in orbit, *J. Geophys. Res.*, *107*(D24), 8213, doi:10.1029/2001JD001439, 2002a.

Nakajima, H., et al., Tangent height registration for the solar occultation satellite sensor ILAS: A new technique for version 5.20 products, *J. Geophys. Res.*, *107*(D24), 8215, doi:10.1029/2001JD000607, 2002b.

Nash, E. R., P. A. Newman, J. E. Rosenfield, and M. R. Schoeberl, An objective determination of the polar vortex using Ertel's potential vorticity, *J. Geophys. Res.*, *101*, 9471–9478, 1996.

Newman, P. A., D. W. Fahey, W. H. Brune, and M. J. Kurylo, Preface to special section: Photochemistry of Ozone Loss in the Arctic Region in Summer (POLARIS), *J. Geophys. Res.*, *104*, 26,481–26,495, 1999.

NOAA, *Northern Hemisphere Winter Summary 1999–2000*, Nat. Weather Serv./Nat. Cent. for Environ. Predict./Clim. Predict. Cent., Camp Springs, Md., 2000a.

NOAA, *Southern Hemisphere Winter Summary 2000*, Nat. Weather Serv./Nat. Cent. for Environ. Predict./Clim. Predict. Cent., Camp Springs, Md., 2000b.

Oltmans, S. J., and D. J. Hofmann, Increase in lower-stratospheric water vapor at a mid-latitude Northern Hemisphere site from 1981 to 1994, *Nature*, *374*, 146–149, 1995.

Oltmans, S. J., H. Vömel, D. J. Hofmann, K. H. Rosenlof, and D. Kley, The increase in stratospheric water vapor from balloonborne, frost point hygrometer measurements at Washington, D.C., and Boulder, Colorado, *Geophys. Res. Lett.*, *27*, 3453–3456, 2000.

Ovarlez, J., Stratospheric water vapor measurement in the tropical zone by means of a frost-point hygrometer on board long-duration balloons, *J. Geophys. Res.*, *96*, 15,541–15,545, 1991.

Ovarlez, J., and H. Ovarlez, Stratospheric water vapor content evolution during EASOE, *Geophys. Res. Lett.*, *21*(13), 1235–1238, 1994.

Pan, L. L., W. Randel, H. Kanzawa, Y. Sasano, S. Massie, H. Nakajima, T. Yokota, and T. Sugita, Variability of polar stratospheric water vapor observed by ILAS, *J. Geophys. Res.*, *107*(D24), 8214, doi:10.1029/2001JD001164, 2002.

Randel, W. J., F. Wu, J. M. Russell III, A. Roche, and J. W. Waters, Seasonal cycles and QBO variations in stratospheric CH_4 and H_2O observed in UARS HALOE data, *J. Atmos. Sci.*, *55*, 163–185, 1998.

Rind, D., E. W. Chiou, W. Chu, S. Oltmans, J. Lerner, J. Larsen, M. P. McCormick, and L. McMaster, Overview of the stratospheric aerosol and gas experiment II water vapor observations: Method, validation, and data characteristics, *J. Geophys. Res.*, *98*, 4835–4856, 1993.

Rosenlof, K. H., et al., Stratospheric water vapor increases over the past half-century, *Geophys. Res. Lett.*, *28*, 1195–1198, 2001.

Rothman, L. S., et al., The HITRAN molecular spectroscopic database and HAWKS (HITRAN atmospheric workstation): 1996 edition, *J. Quant. Spectrosc. Radiat. Transfer*, *60*, 665–710, 1998.

Saitoh, N., S. Hayashida, Y. Sasano, and L. L. Pan, Characteristics of Arctic polar stratospheric clouds in the winter of 1996/1997 inferred from ILAS measurements, *J. Geophys. Res.*, *107*(D24), 8205, doi:10.1029/2001000595, 2002.

Sasano, Y., M. Suzuki, T. Yokota, and H. Kanzawa, Improved Limb Atmospheric Spectrometer (ILAS) for stratospheric ozone layer measurements by solar occultation technique, *Geophys. Res. Lett.*, *26*, 197–200, 1999a.

Sasano, Y., et al., Validation of ILAS version 3.10 ozone with ozonesonde measurements, *Geophys. Res. Lett.*, *26*, 831–834, 1999b.

Sasano, Y., M. Suzuki, T. Yokota, and H. Kanzawa, ILAS for stratospheric ozone layer monitoring: Outline of data processing (version 3.00 and 3.10) and validation experiments, *IEEE Trans. Geosci. Remote Sens.*, *37*, 1508–1516, 1999c.

Solomon, S., Stratospheric ozone depletion: a review of concept and history, *Rev. Geophys.*, *37*, 275–316, 1999.

Stowasser, M., H. Oelhaf, G. Wetzel, F. Friedl-Vallon, G. Maucher, M. Seefeldner, O. Trieschmann, T. von Clarmann, and H. Fischer, Simultaneous measurements of HDO, H_2O and CH_4 with MIPAS-B: Hydrogen budget and indication of dehydration inside the polar vortex, *J. Geophys. Res.*, *104*, 19,213–19,225, 1999.

Sugita, T., et al., Validation of ozone measurements from the Improved Limb Atmospheric Spectrometer (ILAS), *J. Geophys. Res.*, *107*(D24), 8212, doi:10.1029/2001JD000602, 2002.

Suzuki, M., A. Matsuzaki, T. Ishigaki, N. Kimura, N. Araki, T. Yokota, and Y. Sasano, ILAS, the Improved Atmospheric Spectrometer, on the Advanced Earth Observing Satellite, *IEICE Trans. Fundam. Electron. Commun. Comput. Sci.*, *E78-B*, 1560–1570, 1995.

Swinbank, R., and A. O'Neill, A stratosphere-troposphere data assimilation system, *Mon. Weather Rev.*, *122*, 686–702, 1994.

Toon, G. C., JPL Mark IV interferometer, *Opt. Photonics News*, *2*, 19–21, 1991.

Toon, G. C., et al., Comparison of MkIV balloon and ER-2 aircraft measurements of atmospheric trace gases, *J. Geophys. Res.*, *104*, 26,779–26,790, 1999.

Toon, G., B. Sen, J.-F. Blavier, Y. Sasano, T. Yokota, H. Kanzawa, T. Ogawa, M. Suzuki, and K. Shibasaki, Comparison of ILAS and MkIV profiles of atmospheric trace gases measured above Alaska in May 1997, *J. Geophys. Res.*, *107*(D24), 8211, doi:10.1029/2001JD000640, 2002.

Weinstock, E. M., E. J. Hintsa, A. E. Dessler, J. F. Oliver, N. L. Hazen, J. N. Demusz, N. T. Allen, L. B. Lapson, and J. G. Anderson, New fast response photofragment fluorescence hygrometer for use on the NASA ER-2 and the Perseus remotely piloted aircraft, *Rev. Sci. Instrum.*, *65*, 3544–3554, 1994.

Yokota, T., M. Suzuki, O. V. Duvobik, and Y. Sasano, ILAS (Improved Limb Atmospheric Spectrometer)/ADEOS data retrieval algorithms, *Adv. Space Res.*, 393–396, 1998.

Yokota, T., H. Nakajima, T. Sugita, H. Tsubaki, Y. Itou, M. Kaji, M. Suzuki, H. Kanzawa, J. H. Park, and Y. Sasano, Improved Limb Atmospheric Spectrometer (ILAS) data retrieval algorithm for version 5.20 gas profile products, *J. Geophys. Res.*, *107*, doi:10.1029/2001JD000628, in press, 2002.

Zöger, M., et al., Fast in situ stratospheric hygrometers: A new family of balloonborne and airborne Lyman α photofragment fluorescence hygrometers, *J. Geophys. Res.*, *104*, 1807–1816, 1999a.

Zöger, M., A. Engel, D. S. McKenna, C. Schiller, U. Schmidt, and T. Woyke, Balloonborne in situ measurements of stratospheric H_2O, CH_4 and H_2 at midlatitudes, *J. Geophys. Res.*, *104*, 1817–1825, 1999b.

J.-F. Blavier, B. Sen, and G. C. Toon, Jet Propulsion Laboratory, California Institute of Technology, 4800 Oak Grove Drive, Pasadena, CA 91109, USA. (toon@mark4sun.jpl.nasa.gov; sen@mark4sun.jpl.nasa.gov; Jean.F.Blavier@jpl.nasa.gov)

G. E. Bodeker, National Institute of Water and Atmospheric Research-Lauder, Private Bag 50061, Omakau, Central Otago, New Zealand. (g.bodeker@niwa.cri.nz)

C. Camy-Peyret, P. Jeseck, and S. Payan, Laboratoire de Physique Moléculaire et Applications (LPMA), Université Pierre et Marie Curie/CNRS, 4 Place Jussieu, F-75252 Paris Cedex 05, France. (camy@ccr.jussieu.fr; payan@ccr.jussieu.fr; jeseck@ccr.jussieu.fr)

D. G. Johnson and J. H. Park, NASA Langley Research Center, Hampton, VA 23681-2199, USA. (d.g.johnson@larc.nasa.gov; j.h.park@larc.nasa.gov)

K. W. Jucks and W. A. Traub, Harvard-Smithsonian Center for Astrophysics, 60 Garden St., Cambridge, MA 02138, USA. (wtraub@cfa.harvard.edu; kjucks@cfa.harvard.edu)

H. Kanzawa, T. Sugita, H. Nakajima, T. Yokota, and Y. Sasano, National Institute for Environmental Studies, 16-2 Onogawa, Tsukuba, Ibaraki 305-0053, Japan. (kanzawa@nies.go.jp; tsugita@nies.go.jp; hide@nies.go.jp; yoko@nies.go.jp; sasano@nies.go.jp)

H. Oelhaf and M. Stowasser, Institut für Meteorologie und Klimaforschung, Forschungszentrum Karlsruhe, Postfach 3640, D-76021 Karlsruhe, Germany. (hermann.oelhaf@imk.fzk.de; markus.stowasser@imk.fzk.de)

J. Ovarlez, Laboratoire de Météorologie Dynamique (LMD)/CNRS, Ecole Polytechnique, F-91128 Palaiseau Cedex, France. (Joelle.ovarlez@polytechnique.fr)

L. L. Pan, National Center for Atmospheric Research, Boulder, CO 80307, USA. (liwen@ucar.edu)

C. Schiller, Institut für Stratosphaerische Chemie, Forschungszentrum Jülich, D-52425 Juelich, Germany. (c.schiller@fz-juelich.de)

M. Shiotani, Radio Science Center for Space and Atmosphere, Kyoto University, Uji, Kyoto 611-0011, Japan. (shiotani@kurasc.kyoto-u.ac.jp)

M. Suzuki, NASDA/Earth Observation Research Center, 1-8-10, Harumi, Chuou-Ku, Tokyo 104-6023, Japan. (suzuki@eorc.nasda.go.jp)